Shank3 deficiency severely dampens calcium buffer capacity in dopaminergic neurons from the ventral tegmental area

Running Title: Reduced calcium buffer capacity in Shank3-/- dopaminergic neurons

Lulu Lü†[1,2], Yubo Lai†[1], Runfeng Sun†[1], Ruolin Liu§[1], Junhui Lai[1], Mengye Zhu[3], Yunshen Chen[1], Qinglian Liu[4], Lei Zhou*[1]

[1]Institute of Molecular Physiology, Shenzhen Bay Laboratory, Shenzhen, Guangdong 518000, P.R.China;

[2]School of Basic Medical Sciences, Capital Medical University, Beijing 100054, P.R.China;

[3]Department of Pain Medicine, The First Affiliated Hospital of Nanchang University, Jiangxi Medical College, Nanchang University, Nanchang, Jiangxi 330006, P.R.China;

[4]Department of Physiology and Biophysics, School of Medicine, Virginia Commonwealth University, Richmond, VA 23298, USA.

†Contribute equally

*Correspondence to: Lei Zhou: zhoulei@szbl.ac.cn

Acknowledgments

We acknowledge the discussion and technical support from other members of the lab. L. Zhou is supported by fundings from the National Natural Science Foundation of China (#32171150), Shenzhen Bay Laboratory (Startup Fund and Major Program of SZBL), Pearl River Talents Program of Guangdong Province, and Shenzhen Peacock Project. Q. Liu is supported by fundings from Virginia Commonwealth University (CTSA) and NIH (R01GM098592). The authors declare no competing interests.

Lay Summary

SHANK3 is a scaffolding protein highly enriched in the postsynaptic density (PSD) of excitatory synapses. Mutations and deletions of the *SHANK3* gene are the primary risk factor for Phelan-McDermid syndrome (PMS) and autism spectrum disorders (ASD). The links between the genetic alterations in the *SHANK3* gene and the abnormalities at cellular, network, and behavior levels have been unclear. This study uncovered abnormal calcium signaling and action potential firing in dopaminergic neurons. Calcium plays a central role in almost every aspect of neuronal physiology. A definitive link between defects in the SHANK3 protein, the calcium buffering system, and a psychiatric disorder is established for the first time.

Abstract

The intracellular calcium buffer system plays a critical role in shaping the spatiotemporal profile of calcium signaling. In contrast to calcium influx and clearance from the cytosol, our understanding of the calcium buffer system and its role in neuropsychiatric disorders is limited. Shank3 deficiency is a key risk factor for autism and other psychiatric disorders, and many important downstream mechanisms, relating to signaling pathways, cellular physiology and morphology, and neuronal circuitry, have been uncovered. Here we report prominent alterations in the calcium signaling profile of Shank3-/- dopaminergic (DA) neurons in the ventral tegmental area (VTA). Calcium transients from Shank3-/- DA neurons exhibit enhanced amplitudes and faster decay rates. Subsequent proteomic analysis of VTA brain tissue revealed that parvalbumin (PV) expression was significantly downregulated, which was subsequently confirmed by immunostaining results. As PV is an important component of the endogenous calcium buffer system, we employed the added-buffer approach together with 2-photon and ratiometric calcium and demonstrated a reduction in the endogenous calcium buffer capacity (K_E) in Shank3-/- neurons. Therefore, the downregulation of PV protein and the associated decrease in calcium buffer capacity are key pathogenic factors resulting from Shank3 deficiency.

Keywords: Autism, Shank3, calcium buffer capacity, ventral tegmental area, dopaminergic neuron, parvalbumin.

Introduction

Calcium serves as a central second messenger in both excitable cells, such as neurons and muscles, and non-excitable cells (Clapham, 2007; Eisner et al., 2023). The dynamic profile of free calcium ion concentration within the cytosol encodes vital information for numerous physiological processes (Leybaert and Sanderson, 2012; Evans and Blackwell, 2015; Jedrzejewska-Szmek et al., 2023). Much focus has been placed on the influx of calcium ions through cell surface channels and receptors, the release of calcium from internal stores into the cytosol, and the clearance of excess calcium from the cytosol (Enomoto et al., 2017). Malfunctions in any of these steps have serious consequences and may contribute to the development of various neuropsychiatric diseases (Nanou and Catterall, 2018; Pchitskaya et al., 2018). However, one critical aspect of cytosolic calcium signaling is often overlooked: approximately 99% of cytosolic calcium is bound to calcium-binding proteins (Brinley, 1978; Matthews and Dietrich, 2015; Schwaller, 2020). Therefore, components of the calcium buffer system exert a profound influence on the spatiotemporal profile of calcium signaling: they serve as essential protective absorbents against toxic levels of calcium, but they also directly release calcium when free calcium concentrations are low (Fakler and Adelman, 2008). Notably, low expression of PV, a 12 kDa calcium-binding protein, has been reported in neurodegenerative diseases and autism spectrum disorders (ASD) (Jung et al., 2019; Filice et al., 2020; Janickova et al., 2020; Contractor et al., 2021; Ruden et al., 2021). During the progress of both acute and long-term neuropsychiatric disorders, neurons of intrinsically high PV expression often exhibit increased metabolic and translational activity, making them more vulnerable to pathological damage (Hu et al., 2014; Ruden et al., 2021; Tang et al., 2021; Kumar et al., 2024). However, a direct connection between abnormalities in calcium buffering capacity and nervous system disorders has yet to be established.

The *SHANK3* gene encodes an important scaffolding protein highly enriched in the postsynaptic density (PSD) of glutamatergic synapses (Durand et al., 2007; Leblond et al., 2014). The full-length Shank3 protein contains highly conserved domains that mediate protein-protein interactions, including an Ankyrin repeat domain, an SH3 domain, and a PDZ domain, followed by a proline-rich region and a SAM domain. Multiple intragenic promoters within the *SHANK3* gene, along with alternative exon splicing, resulting in a complex cohort of SHANK3 isoforms (Wang et al., 2014). Beyond PSD, Shank3 is also expressed in the soma, axons, presynaptic terminals, and even the nucleus, but the function of Shank3 in these areas remains to be clarified (Wang et al., 2014; Halbedl et al., 2016b; Han et al., 2016).

Mutations in the *SHANK3* gene have been linked to several brain disorders, including Phelan-McDermid syndrome (PMS), ASD, schizophrenia, mania, and dementia. Despite these associations, many gaps exist in understanding how genetic defects translate into behavioral phenotypes in *SHANK3*-related pathology. To address this, dozens of Shank3 knockout mouse models of various designs have been developed, and to varying extents, they have recapitulated the neurological symptoms observed in human patients (Peca et al., 2011; Bariselli et al., 2016; Wang et al., 2016; Drapeau et al., 2018; Delling and Boeckers, 2021). At the cellular level, Shank3 deficiency causes abnormalities in the morphology of neuronal structures, the surface expression and localization of various receptors and ion channels, synaptic transmission and plasticity, and neurophysiological activities at the cellular and circuit levels. Among the plethora of ion channels expressed in neurons, the downregulation of HCN channel expression and function of HCN channels is considered a primary consequence of Shank3 deficiency (Yi et al., 2016; Zhu et al., 2018). This downregulation of HCN channels directly causes abnormal neuronal excitability, including aberrant action potential firing, negatively shifted resting membrane potential, and increased input resistance (Santoro and Shah, 2020; Combe and Gasparini, 2021).

The HCN channelopathy resulting from Shank3 deficiency has been studied in two types of excitatory neurons: the pyramidal neurons in the hippocampus and the thalamocortical neurons in the thalamus (Yi et al., 2016; Zhu et al., 2018). Here we characterized the DA neurons in the VTA. Most DA neurons in the brain are densely distributed in the VTA, which harbors neuronal circuits important for the reward system (Schultz et al., 1997; Cohen et al., 2012; Morales and Margolis, 2017). In Shank3-/- DA neurons, we identified abnormalities in action potential firing and calcium signaling profile and established the link between Shank3 deficiency and downregulation of cytosolic calcium buffering capacity.

Materials and Methods

Ethical approval

All animal experiments were approved by the IACUC Committee of Shenzhen Bay Laboratory. C57BL/6J mice were used in the current study. The number of animals and as well as procedures involving pain were minimized in compliance with regulations. Animals were subjected to regular veterinary care on a routine basis. The Center for Research Animal Resources was available 24 hours for any case in which veterinary care or consultation was required. Mice were housed in a standard 12-hour light/dark cycle, with free access to food and water. The Shank3 knockout mice were purchased from The Jackson Laboratory (B6.Cg-*Shank3*$^{tm2.1Bux}$/J, Stock No: 017688; jax.org).

Acute brain slice preparation and whole-cell patch-clamp recording

Coronal brain slices were prepared from mice 3-6 weeks old of either sex. In brief, mice were deeply anesthetized by intraperitoneal injection of 1.25% Tribromoethanol (avertin; 0.2 mL/10 g body weight) and then transcardially perfused through the ascending aorta with preoxygenated (95% O2 and 5% CO2) and ice-cold sucrose-based artificial cerebrospinal fluid (sucrose-ACSF). Brain slices of 300 mm thickness were prepared using a vibratome (VT1200S Leica) at 4°C. Slices were incubated first at 34°C for 30 min in standard ACSF and subsequently kept at room temperature for at least 1 hour prior to recording.

Brain slices were perfused continuously in the recording chamber with pre-warmed (34°C) carbonated standard ACSF at a rate of 2-3 ml/min. Visually identified healthy neurons were recorded with glass pipettes (4-6 MΩ) filled with the internal solution. Voltage and current signals recorded from neuron soma were amplified by MultiClamp 700B (Molecular Devices), digitized by an A/D converter (NI USB-6341, National Instruments) and acquired by WinWCP (Dr. John Dempster, University of Strathclyde). All electrophysiological data is collected at a sampling frequency of 20 kHz, with the amplifier filter set at 10 kHz. Resting membrane potential and input resistance data are recorded immediately after membrane rupture. Action potential and other signals were recorded from neurons that have remained stable for at least 5 minutes after membrane rupture. Data were offline converted to Axon file format and analyzed by Clampfit (Molecular Devices). Neurons with an RMP more negative than -50 mV and the peak of action potential (AP) passing 0 mV were selected for recording. Input resistance (Rin) was measured at RMP based on the change in membrane potential in response to a 10 pA current injection (500 msec). APs were elicited with depolarizing current pulses according to the description in the text.

Two-Photon Calcium Imaging

An Olympus two-photon microscope (FVMPE-RS) with custom IR-DIC was used for calcium imaging in neuron soma and dendrites. A femtosecond pulsed laser (Spectra-Physics) at 810 nm was used for calcium dye and AF594 excitation. Fluorescence signals were collected by a 25X water immersion objective lens for multi-photon recording (ND 1.05, WD 2.0 mm, 400-1600 nm applicable, Olympus) and recorded through the green channel (495-540 nm emission filter) and the red channel (575-645 nm filter) by two GaAsP PMTs (RNDD3G; RNDD4G). The TTL signal generated by the WinWCP program was used to trigger the recording of time-lapse images at the frequency of 25 frames per second. To minimize photobleaching, the laser power was typically set in the range of 3.5 - 5%. To approach optimal intensity of each frame, Galvan instead of Resonant scanner was used and the exposure time was in the range between 10 and 20 μs/pixel. The size

of ROI was adjusted so that the frame rate can reach 25 Hz. The fluorescence intensity of each ROI was monitored on-line during each experiment and analyzed off-line using Clampfit. Background fluorescence was subtracted by manual selection of an area away from the electrode, soma, and dendrites. Optical and electrical recordings were carried out simultaneously. Burst firing of TRN neurons was triggered by 3 or 4 current injections (500 pA / 10 msec duration / 1 second interval) at the RMP of -70 mV. No averaging and filtering were applied to the fluorescence signal during data analysis.

Ratiometric calcium imaging

Fura-8, a high-affinity ratiometric calcium indicator, was alternatively excited by two LED light sources, 365 nm and 410 nm. Fluorescence signals were collected by a 40X water immersion lens (CFI Apo NIR 40X W, Nikon), passed through the filter cube, and detected by a back-illuminated sCMOS camera (Dhyana 400BSI by Tucsen). The exposure time and frame rate were set at 20 msec and 40 Hz, respectively. A total of 390 images were recorded at 40 Hz (195 data points at 20 Hz) for each episode. ImageJ and Clampfit were used for data analysis. TTL signals generated by the WinWCP program were used to synchronize the electrophysiology amplifier (AM2400, A-M Systems), the LED light sources, and the sCMOS camera.

The procedure for calculating the free calcium centration was based on published studies (Zhou and Neher, 1993; Maravall et al., 2000; Delvendahl et al., 2015; Helmchen and Tank, 2015). The endogenous calcium buffer power was estimated by the “added buffer” approach where exogenous calcium buffers at different capacities compete with endogenous buffers. The analysis involves the calculation of fluorescence intensity (F_i) and the effective binding constant (K_{eff}), as outlined in equations (1) and (2) as described below:

Step 1: calculation of intracellular fluorescence intensity Fi

F_i can be calculated using the following formula:

$$Fi = F1 + \alpha F2 \qquad (1)$$

, where F1 and F2 represent the fluorescence intensity measured at 365 nm and 410 nm, respectively, and α represents the isocoefficient so that F_i is independent of calcium concentration. The background fluorescence intensity was subtracted from all measurements. F_i serves as an indicator independent of calcium concentration and can reflect the concentration of Fura-8 inside the neuron. As the whole-cell patch-clamp recording progresses after the rupture of the membrane seal, the Fi value gradually increases.

Step 2: calculation of the effective binding constant K_{eff} of Fura-8

$$K_{eff} = K_D \frac{R_{\max} + \alpha}{R_{\min} + \alpha} \quad (2)$$

, where K_D represents the dissociation constant of Fura-8 (260 nM), Rmax and Rmin are the maximum and minimal ratios of intensity measured using an electrode solution containing 10 mM $CaCl_2$ and 10 mM EGTA, respectively.

Step 3: calculation of intracellular free calcium ion concentration

$$[Ca^{2+}] = K_{eff} \frac{R - R_{\min}}{R_{\max} - R} \quad (3)$$

, where R represents the ratio of fluorescence intensities excited by 365 nm and 410 nm light. The resting calcium ion concentration $[Ca2+]_{rest}$ and the peak calcium ion concentration $[Ca2+]_{peak}$ after induced AP firing can be obtained from eq. 3.

Step 4: calculation of calcium buffer capacity K_B

After the rupture of the membrane seal, the concentration of Fura-8 - as well as the corresponding calcium buffer capacity K_B - gradually increases in the cytosol. $[B]_t$ represents the concentration of the calcium dye inside the neuron and can be calculated by the following equation:

$$[B]_t = [B]_p \bullet F_i / F_{i\infty} \quad (4)$$

, where [B]p is the total concentration of Fura-8 in the electrode solution (50 μM), F_i represents the F_i value at a given time and can be calculated from formula (1), and $F_{i\infty}$ represents the F_i value when Fura-8 reaches equilibrium inside the neuron (typically after 20 minutes), also calculated from formula (1).

The K_B can be calculated by:

$$K_B = \frac{[B] \bullet K_D}{([Ca^{2+}]_{rest} + K_D)([Ca^{2+}]_{peak} + K_D)} \quad (5)$$

, where K_D is the dissociation constant of Fura-8 (260 nM); $[Ca2+]_{rest}$ and $[Ca2+]_{peak}$ can be obtained from formula (3).

Step 5: calculation of decay time constant of calcium transients

After rupturing the cell membrane, the exogenous calcium buffer power K_B increases as Fura-8 gradually enters the neuron. Increased calcium buffer power tends to decrease the amplitude of the calcium transients and increase the time constant for the decay phase. The decay time constant τ of the calcium transients can be obtained using Clamfit software. The relationship between K_B and τ at different time points can be fitted into a linear equation:

$$\tau = \frac{1 + K_B + K_E}{\gamma} \quad (6)$$

, where τ is obtained from Clamfit software, K_B is calculated using formula (5), and the negative x-axis intercept provides an estimate of the endogenous buffer capacity K_E. Following this procedure,

we can determine the endogenous calcium buffer capacity of neurons from WT and SHANK3-/- mice.

Solutions used (all in mM):

Heart perfusion and brain slice preparation solution: Sucrose, 220; KCl, 2.5; NaH_2PO_4, 1.25; $MgSO_4$, 6; $CaCl_2$, 0.5; $NaHCO_3$, 25; Glucose, 20; ascorbic acid, 0.4; Na Pyruvate, 2.

Brain slice incubation and recording solution: NaCl, 125; KCl, 2.5; NaH_2PO_4, 1.25; $MgSO_4$, 2; $CaCl_2$, 2; $NaHCO_3$, 25; Glucose, 20; Ascorbic acid, 0.4; Na Pyruvate, 2.

Standard electrode solution: KGluconate, 130; KCl, 5; $MgSO_4$, 2; Creatine Phosphate, 5; ATP, 1; GTP, 0.3; HEPES, 10 ; EGTA 0.5.

Electrode solution for calcium imaging: KGluconate, 130; KCl, 5; $MgSO_4$, 2; Creatine Phosphate, 5; ATP, 1; GTP, 0.3; HEPES, 10.

Reagents used:

For two-photon calcium imaging, two calcium indicators were used: Fluo-5F (pentapotassium salt) and Fluo-4 (pentapotassium salt). To trace neuronal soma and dendrites, a red fluorescent dye Alexa Fluor™ 594 (commonly abbreviated as AF 594) was used.

DHPG, an agonist of metabotropic glutamate receptors; Caffeine, an agonist of ryanodine receptors (RyRs); Ryanodine, an antagonist of RyRs; Isradipine, an antagonist of L-type voltage-gated calcium channels.

Immunofluorescence Staining

Mice under anesthesia were transcardially perfused with approximately 20 ml of ice-cold PBS solution, followed by 20 ml of pre-cooled 4% paraformaldehyde. Then the brain tissue was dissected out and immersed in 4% paraformaldehyde for overnight fixing, followed by soaking with 30% sucrose for cryoprotection and then frozen in OCT medium.

Brain slices of 25 μm were prepared using a Leica cryostat and then washed in 0.1% PBST for 3 times and 0.3% PBST for 20 minutes. After blocking with PBST and 10% goat serum for 1 hour, brain slices were incubated with primary antibodies (chicken anti-Tyrosine Hydroxylase (TH) antibody for labeling dopamine neurons and rabbit anti-PV antibody for PV protein labeling, both diluted 1:1000) at 4°C overnight. After rinsing three times, brain slices were incubated with secondary antibodies in the dark (594-goat anti-chicken, ab150176, Abcam, 1:1000; 488-goat anti-rabbit, ab150077, Abcam, 1:1000) at room temperature for 1 hour. After extensive rinsing, brain slices were mounted with sealing agent DAPI-Aqueous (ab104139, Abcam). Parameters of the confocal microscope, especially the laser power and detector gain, were pre-adjusted to minimize photobleaching. The same set of parameters were used in the data collection for parallelly processed WT and Shank3-/- mutant samples. After raw image to TIFF format (16 bit), ImageJ was

used for data analysis. For each brain slice, the VTA region was manually selected (Freehand selections) and cell bodies were registered with TH signal (red channel) as the guidance. The size parameter was set as 0.05-3 inch2 (Analyze Particles). Then the ROI outputs were used to measure the PV signal (green channel) of the selected cell bodies. For each brain slice, we obtain the total number of TH+ neurons and the average PV signal intensity. Final statistics were based on results of all brain slices used in data analysis (**Fig. S3A-B**). To compare PV expressions between WT and Shank3+/- samples, we first converted the raw TIFF image (whole image selection) to an Excel file containing the X-Y coordinates and intensity of each pixel. With TH signal intensity as guidance (red channel, >50 a.u.), positive pixels were pooled together and their green channel intensities, corresponding to PV expression, were used in histogram analysis (**Fig. S3C-E**). Images from the mouse brain atlas, including the *in-situ* hybridization data of PV, were shown for reference purposes (**Fig. S3F**).

Proteomics Analysis via Mass Spectrometry

Mouse Brain Tissue Collection

A total of 9 WT mice and 9 Shank3-/- mice, each aged between 3-6 weeks and born from the same litter, were used in the experiments. The mice under anesthesia were transcardially perfused with pre-chilled PBS solution. The brain tissue was quickly trimmed and mounted on a sample holder for slicing. Coronal slices were prepared in slushy PBS using VT1200S with the following parameters: speed 0.06 mm/s, amplitude 0.85 μm, and thickness 400 μm. The VTA region was carefully dissected from the slices under a stereo-dissection microscope and saved in Eppendorf tubes.

Total Protein Extraction

The brain tissue was first rinsed in pre-chilled PBS and then mixed with pre-chilled membrane and cytoplasmic protein extraction buffer: Buffer A (C510005, Sangon Biotech) supplemented with 1 μl DTT, 10 μl PMSF, 1 μl protease inhibitor, and 5 μl phosphatase inhibitor. Stainless steel beads (3 mm) were added into each EP tube for tissue homogenization, with a tissue grinder of the setting of 60 HZ for 60 seconds, followed by a 15-second pause, for a total of 3 cycles at -10°C. Then the homogenized tissue was centrifuged at 4°C, 3000 rpm for 3 minutes. Next, the tissue was further homogenized by an ultrasonic cell disruptor (KZ-5F-3D, Servicebio Inc), with the protocol of 30 seconds on, 60 seconds off, for a total of 5 repeats at 25% power. The homogenized solution was centrifuged at 4°C, 4100 rpm for 10 minutes. The supernatant was collected and subjected to a second centrifugation step at 4°C, 13000 rpm for 90 minutes. The supernatant, corresponding mostly to the cytoplasmic soluble fraction, was collected and stored on ice. The pellet was then mixed with pre-chilled Buffer B (C510005, Sangon Biotech; 1 ml supplemented with 1 μl DTT, 10

304 µl PMSF, 1 µl protease inhibitor, and 5 µl phosphatase inhibitor), followed by extensive vortex and
305 centrifugation at 4°C, 13000 rpm for 10 minutes. The supernatant, corresponding mostly to the
306 membrane fraction, was transferred to a pre-chilled clean microcentrifuge tube. This is the
307 membrane protein. The cytoplasmic and membrane proteins were mixed and stored at -80°C or
308 proceeded to the protein precipitation step.
309
310 *Protein Precipitation*
311 To precipitate proteins, 250 µl of a methanol/chloroform solution (4:1 ratio) was added to 200 µl of
312 the samples and incubated at -20°C for 2.5 hours. The precipitated proteins were pelleted by
313 centrifugation at 17,000 xg for 10 min at 4°C. The protein pellets were washed three times with 1
314 ml methanol (pre-chilled to -20°C) to remove chloroform and subsequently dried. Each sample was
315 resuspended and dissolved in 100 µl of 50 mM ammonium bicarbonate solution using sonication.
316
317 *Mass Spectrometry Analysis*
318 After protein concentration determination using the bicinchoninic acid (BCA) assay, each sample
319 was adjusted to the same concentration (> 1 µg/µl) using 50 mM ammonium bicarbonate. Urea
320 was added to each sample to a final concentration of 2-4 M to fully solubilize the proteins. To reduce
321 disulfide bonds, TCEP was added to a final concentration of 10 mM, and the samples were
322 incubated at 37°C for 1 hour. Iodoacetamide was then added to a final concentration of 20 mM to
323 modify cysteine residues and prevent disulfide bond formation. After diluting the samples 3 times
324 with 50 mM ammonium bicarbonate, trypsin was added to a final concentration of 4.8 ng/µl, and
325 the samples were incubated at 37°C for 16-18 hours to allow complete digestion by trypsin. Typical
326 protein concentration was in the range of 0.1-5 µg/µl. Thermo Hypersep C18 columns were used
327 for desalting. After drying to remove acetonitrile from the C18 column elution, the final samples
328 were dissolved in 0.1% formic acid. The concentration of each sample was adjusted to 250 ng/µl.
329 Samples were then subjected to mass spectrometry analysis using an Exploris 480 Hybrid
330 Quadrupole-Orbitrap Mass Spectrometer.
331
332 **Expression and Purification of mouse parvalbumin (PV)**
333 The open-reading frame of mouse PV was amplified and cloned into the pSMT3 vector (a generous
334 gift from Dr. Christopher Lima, MSK Cancer Center). After the DNA sequence was confirmed by
335 sequencing, the resulting pSMT3-PV plasmid was transformed into the *E. coli* BL21(DE3) strain for
336 expression. Expression was induced at 30 °C for 8 hours in LB Miller medium by adding IPTG to a
337 final concentration of 1 mM. The mouse PV was expressed as a Smt3 fusion protein with a His6
338 tag at the N-terminus. A HisTrap column (Cytiva) was used for the first step of purification, with
339 buffers containing 25 mM Hepes-NaOH, pH 7.5, 300 mM NaCl, 10% glycerol, and 1 mM TCEP.

After incubating with the Ulp1 protease overnight, the Smt3 tag was cleaved off. A second HisTrap was applied to remove the Smt3 tag. The resulting protein was > 95% pure and concentrated to > 10 mg/ml. After aliquoting to 50 µl per tube, the purified PV protein was flash-frozen and stored in a -80 °C freezer.

Statistics

All statistical tests were performed using the program of OriginPro. Data are presented as mean ± SEM. Statistical significance was assessed with unpaired student t test. $P < 0.05$ was considered statistically significant, and significance is indicated as follows: ***, $P < 0.001$; **, $P < 0.01$; *, $P < 0.05$. P-value is provided in figure legends.

Results

Abnormal neuronal excitability and faster somatic calcium signal clearance in Shank3-/- VTA DA neurons

We started with electrophysiological characterization of VTA DA neurons from WT and Shank3-/- mice (**Fig. 1A, 1B**). To evoke action potential (AP) firing, a series of current injections, at the interval of +50 pA, were applied to the neuron. In Shank3-/- DA neurons, we observed significant decreases in the number, half-width, and half-amplitude of AP (**Fig. 1C-1E**). The resting membrane potential (RMP) of the Shank3-/- neuron was slightly negative than that of WT, whereas the input resistance was comparable (**Fig. 1F**).

Calcium plays a key role in bridging neuronal excitability to various physiological processes and is the most important second messenger in neurons. Next, we examined the profile of somatic calcium signaling using 2-photon calcium imaging. Calcium dyes (200 µM Fluo-4) were loaded into the neuron through whole-cell recording pipettes, with four short current injection pulses at time intervals to trigger AP firing (**Fig. 2A-2B**). Two calcium dyes with different K_D values were used in the experiments: Fluo-4, a high-affinity dye with a K_D of approximately 345 nM, and Fluo-5F, a low-affinity dye with a K_D of approximately 2.3 µM. In Shank3-/- DA neurons, the amplitudes of the calcium transients were consistently higher whereas the decay proceeded much faster compared to WT neurons (**Fig. 2C-2F**).

Altered dendritic calcium signaling in Shank3-/- VTA DAneurons

Next we examined the profile of dendritic calcium signaling using two-photon calcium imaging (**Fig. 3A**). We started from Fluo-4, a high-affinity calcium dye with a K_D ~345 nM. After membrane break-in, we waited ~20 minutes before collecting images of dendritic fluorescence signal. We chose three spots along the same dendritic trunk, at distances of 50, 100, or 150 mm from the soma, and recorded the calcium transients in response to the same set of somatic current injections as used above. Analysis of the time constant and the amplitude of the calcium transients revealed interesting changes consistent with those observed at the soma: faster decay and increased amplitude of dendritic calcium transients in Shank3-/- neurons (**Fig. 3B-3C**). In addition, we tested Fluo-5F, a low-affinity calcium dye with a K_D of ~2.3 μM (**Fig. 3D**). From the soma to three spots along the dendritic trunk, the calcium transients of the Shank3-/- DA neuron showed a faster decay (**Fig. 3E-3F**).

Reduced PV expression in Shank3-/- VTA neurons revealed by mass spectrometry and immunostaining

To explore the molecular basis of the faster calcium clearance in Shank3-/- neurons, we started with a pharmacological approach by perturbing the relevant calcium influx and clearance pathways. However, the results could not explain the faster decay of calcium transients observed in Shank3-/- neurons (**Fig. S1**). We then utilized a systematic proteomics approach to evaluate the proteins that show abnormal expression upon Shank3 deficiency. To improve the specificity for the VTA region, we dissected the brain tissue in the VTA region of WT and Shank3-/- mice and subjected the protein extraction to mass spectrometry analysis (**Fig. 4A**). Among the 4882 identified proteins, 132 differentially expressed proteins were identified ($P<0.05$), of which 86 were upregulated and 46 were downregulated (**Fig. 4B**). We then subjected the mass-spec results to clustering, gene ontology (GO), and KEGG pathway analysis (**Fig. 4C-D; S2**). Among the 132 differentially expressed proteins, 29 proteins were found to be closely related to cytoskeletal protein and cell metabolism and development by cluster analysis. Interestingly, GO analysis revealed that the proteins affected by Shank3 deficiency function in regulating the cytoskeleton and associated channels and receptors on the membrane. These structural proteins may contribute to biological processes such as epidermal development and differentiation. The KEGG analysis identified 15 pathways, including metabolic pathways, reactive oxygen species, and neuropsychiatric diseases such as Huntington's disease.

As revealed by mass-spec analysis, PV is at the top of the list of proteins showing reduced expression in the Shank3-/- VTA region. PV is an important calcium-binding protein and critically regulates the spatial and dynamic profile of intracellular calcium. Reduced levels of PV protein could decrease the capacity of calcium buffer, which in theory leads to an increase in calcium

transient amplitude and an acceleration of the decay phase (Eisner et al., 2023). To confirm the mass spectrometry results, we performed immunostaining of PV proteins from fixed brain slices (**Fig. 4E**). Brain slices were collected from paired littermates and processed in parallel during the staining and imaging steps. Tyrosine hydroxylase (TH), a marker for DA neurons, was stained and shown in red, while PV was stained in green. The composite images of the soma of VTA DA neurons showed a dramatic difference between the WT and Shank3-/- samples, with the WT sample showing a yellowish color, whereas the Shank3-/- sample remained red, indicating reduced expression of PV (**Fig. 4F-4H; S3A-S3B**). Interestingly, PV expression in Shank3+/- heterozygote mice also showed significant decreases, as revealed by a pixel-based quantitative intensity analysis guided by TH signals (**Fig. S3C-E**). Notably, the expression level of PV in DA neurons is clearly lower than the “PV+” neuron from nearby regions, including substantia nigra and midbrain reticular nucleus, which is consistent with the in-situ hybridization data (**Fig. S3F**). In addition, Shank3-/- PV+ neurons in the cortex exhibited a significant decrease in PV expression (**Fig. S4**).

Decreased calcium buffer capacity in Shank3-/- VTA DA neurons

PV is a critical component of the endogenous calcium buffering system. We were intrigued by the greatly reduced expression of PV in Shank3-/- neurons as shown above. We set out to quantify the capacity of the calcium buffering system using the “added buffer” approach. The cytosolic calcium buffer capacity critically determines the amplitude and the decay time constant of calcium transients. As an “added perturbation” to the endogenous calcium buffer system, calcium dyes loaded into the neuron tend to decrease the amplitude and increase the decay time constant of calcium transients, respectively, which helps the extrapolation of endogenous calcium buffer capacity. We started with 2-photon calcium imaging based on a single wavelength dye, and to improve the accuracy of the measurements, corroborated the results with radiometric calcium measurements.

We started from Fluo-4 and the 2-photon calcium imaging setup to quantify the endogenous K_E (**Fig. 5A**). A series of short current injections (2 nA, 2 msec, 2 Hz), was used to evoke AP at fixed time points. The corresponding calcium transients were recorded within 30 minutes after membrane break-in (**Fig. 5B-5C**). As indicated by the fluorescence of AF594, the concentration of calcium dye steadily increased and eventually reached equilibrium within 20-30 minutes (**Fig. 5D**). Corresponding to the time-dependent increase in the buffer capacity of Fluo-4 (K_B), a significant slowdown in calcium transient decay was observed (**Figs. 5E**). Linear regression fitted to the dataset of τ-K_B revealed the relative value of the endogenous calcium buffer, K_E (**Fig. 5F**). As expected, the K_E value of Shank3-/- DA neurons is smaller than that of the WT neurons by approximately 23 (**Fig. 5G**).

Next, we used Fura-8, an improved version of the widely used ratiometric calcium dye Fura-2, on a home-built imaging system based on a back-illuminated sCMOS camera (**Fig. 6A**). Fura-8 was alternately excited by 365 and 410 nm light, with the corresponding fluorescence intensity showing opposite changes during a calcium transient (**Fig. 6B-6D**). After the membrane break-in, the calcium dye in the recording pipette began to diffuse into the neuron, eventually reaching equilibrium in approximately 20 minutes. Compared to the calcium transients recorded from WT DA neurons, the Shank3-/- calcium signal showed increased amplitude and faster decay, indicating the reduced calcium buffer capacity (**Fig. 6E**). To quantify the impacts on endogenous calcium buffer capacity, we used the "added buffer" approach by tracking changes in calcium transients for 12 minutes and subjecting collective τ measurements to linear regression analysis (**Figs. 6F-6G**). Averaged results based on measurements from a total of 14 cells revealed that the K_E value of Shank3-/- is reduced by approximately 61 compared to that of WT (**Fig. 6H**).

Discussion

SHANK3 deficiency is a highly penetrant monogenic risk factor for ASD and several other neuropsychiatric disorders. The connections between genetic defects in the *SHANK3* gene and the resulting behavior phenotypes remain unclear. Although Shank3 is known to be a canonical synaptic protein, its role in other neuronal structures, such as the soma and dendrites, is underappreciated (Wang et al., 2014; Halbedl et al., 2016a). Previous research suggested that the primary consequence of Shank3 deficiency is the effect on neuronal excitability, mediated by HCN channelopathy. In the current study of Shank3-/- VTA dopaminergic neurons, we discovered changes in AP firing and an intriguingly fast decay of calcium transients. Significantly reduced PV expression, and consequently reduced calcium buffer capacity, were responsible for the abnormal calcium signaling. Thus, this study extended our understanding of the downstream events of Shank3 deficiency and highlighted the critical role of calcium buffer capacity in related neuropsychiatric disorders.

The majority of DA neurons in the brain are concentrated in the VTA and surrounding regions. It has been proposed that the hypoactivity in DA neurons directly contributes to the maturation of the corresponding circuits during development, thereby underpinning the behavior phenotypes observed in autistic patients (Bariselli et al., 2016; Bariselli et al., 2018). Our electrophysiological characterization of Shank3-/- VTA DA neurons revealed reduced AP firing, shorter AP half-widths, and negatively shifted RMP.

In addition, the calcium transients in Shank3-/- VTA DA neurons exhibit an abnormally fast decay. The spatiotemporal profile of calcium signaling is strongly influenced by the intracellular calcium buffering system. Reduced buffer capacity tends to increase the immediate peak of calcium transients, as the sudden influx of calcium ions quickly overwhelms the intracellular buffers. This transient increase in free calcium could enhance the opening of nearby channels such as the BK potassium channel, potentially contributing to abnormalities in AP shape and firing in Shank3-/- neurons (Hou et al., 2016). During the decay phase, which lasts tens to hundreds of milliseconds, reduced calcium buffer capacity allows free calcium ions to have more opportunities to interact with the clearance system, resulting in faster clearance of intracellular free calcium. Additionally, reduced PV expression limits its capacity as an important source of calcium during the decay phase (Collin et al., 2005; Franconville et al., 2011). In Shank3-/- neurons, this faster decay may limit the spatial scale of cytosolic calcium increases, thereby dampening longer-range events such as SK channel opening or increases in calcium concentration in subcellular structures or organelles (Ma et al., 2023). To further validate the relationship between calcium buffer capacity and the profile of calcium transients, we compensated for the reduced PV expression in Shank3-/- DA neurons by adding additional EGTA (350 μM; **Fig. S5**) or purified recombinant PV protein (5 μM; **Figs. S6, S7**), in addition to Fluo-5F (250 μM) in the pipette solution. As expected, we observed a significant increase in the decay time constant and a decrease in the amplitude of the calcium transients.

In conclusion, our study broadens the understanding of Shank3 deficiency beyond the previously reported HCN channelopathy to include abnormalities in calcium signaling (**Fig. 7**). We discovered reduced PV expression and the corresponding decreases in calcium buffering capacity in Shank3-/- VTA DA neurons. Abnormal calcium buffering capacity has been implicated in several neuropsychiatric disorders, and here our study of Shank3-/- VTA DA neurons provides crucial evidence for this connection. Clinical treatments targeting calcium buffer capacity may represent a novel therapeutic avenue not only for ASD but also for other neuropsychological disorders.

References

Bariselli S, Contestabile A, Tzanoulinou S, Musardo S, Bellone C (2018) SHANK3 Downregulation in the Ventral Tegmental Area Accelerates the Extinction of Contextual Associations Induced by Juvenile Non-familiar Conspecific Interaction. Front Mol Neurosci 11:360.

Bariselli S, Tzanoulinou S, Glangetas C, Prevost-Solie C, Pucci L, Viguie J, Bezzi P, O'Connor EC, Georges F, Luscher C, Bellone C (2016) SHANK3 controls maturation of social reward circuits in the VTA. Nat Neurosci 19:926-934.

Brinley FJ, Jr. (1978) Calcium buffering in squid axons. Annu Rev Biophys Bioeng 7:363-392.

Clapham DE (2007) Calcium signaling. Cell 131:1047-1058.

Cohen JY, Haesler S, Vong L, Lowell BB, Uchida N (2012) Neuron-type-specific signals for reward and punishment in the ventral tegmental area. Nature 482:85-88.

Collin T, Chat M, Lucas MG, Moreno H, Racay P, Schwaller B, Marty A, Llano I (2005) Developmental changes in parvalbumin regulate presynaptic Ca2+ signaling. J Neurosci 25:96-107.

Combe CL, Gasparini S (2021) I(h) from synapses to networks: HCN channel functions and modulation in neurons. Prog Biophys Mol Biol 166:119-132.

Contractor A, Ethell IM, Portera-Cailliau C (2021) Cortical interneurons in autism. Nat Neurosci 24:1648-1659.

Delling JP, Boeckers TM (2021) Comparison of SHANK3 deficiency in animal models: phenotypes, treatment strategies, and translational implications. J Neurodev Disord 13:55.

Delvendahl I, Jablonski L, Baade C, Matveev V, Neher E, Hallermann S (2015) Reduced endogenous Ca2+ buffering speeds active zone Ca2+ signaling. Proc Natl Acad Sci U S A 112:E3075-3084.

Drapeau E, Riad M, Kajiwara Y, Buxbaum JD (2018) Behavioral Phenotyping of an Improved Mouse Model of Phelan-McDermid Syndrome with a Complete Deletion of the Shank3 Gene. eNeuro 5.

Durand CM et al. (2007) Mutations in the gene encoding the synaptic scaffolding protein SHANK3 are associated with autism spectrum disorders. Nat Genet 39:25-27.

Eisner D, Neher E, Taschenberger H, Smith G (2023) Physiology of intracellular calcium buffering. Physiol Rev 103:2767-2845.

546 Enomoto M, Nishikawa T, Siddiqui N, Chung S, Ikura M, Stathopulos PB (2017) From Stores to
547 Sinks: Structural Mechanisms of Cytosolic Calcium Regulation. Adv Exp Med Biol 981:215-
548 251.
549 Evans RC, Blackwell KT (2015) Calcium: amplitude, duration, or location? Biol Bull 228:75-83.
550 Fakler B, Adelman JP (2008) Control of K(Ca) channels by calcium nano/microdomains. Neuron
551 59:873-881.
552 Filice F, Janickova L, Henzi T, Bilella A, Schwaller B (2020) The Parvalbumin Hypothesis of Autism
553 Spectrum Disorder. Front Cell Neurosci 14:577525.
554 Franconville R, Revet G, Astorga G, Schwaller B, Llano I (2011) Somatic calcium level reports
555 integrated spiking activity of cerebellar interneurons in vitro and in vivo. J Neurophysiol
556 106:1793-1805.
557 Halbedl S, Schoen M, Feiler MS, Boeckers TM, Schmeisser MJ (2016a) Shank3 is localized in axons
558 and presynaptic specializations of developing hippocampal neurons and involved in the
559 modulation of NMDA receptor levels at axon terminals. J Neurochem 137:26-32.
560 Halbedl S, Schoen M, Feiler MS, Boeckers TM, Schmeisser MJ (2016b) Shank3 is localized in axons
561 and presynaptic specializations of developing hippocampal neurons and involved in the
562 modulation of NMDA receptor levels at axon terminals. J Neurochem 137:26-32.
563 Han QJ, Kim YH, Wang XM, Liu D, Zhang ZJ, Bey AL, Lay M, Chang W, Berta T, Zhang Y, Jiang YH, Ji
564 RR (2016) SHANK3 Deficiency Impairs Heat Hyperalgesia and TRPV1 Signaling in Primary
565 Sensory Neurons. Neuron 92:1279-1293.
566 Helmchen F, Tank DW (2015) A single-compartment model of calcium dynamics in nerve terminals
567 and dendrites. Cold Spring Harb Protoc 2015:155-167.
568 Hou P, Xiao F, Liu H, Yuchi M, Zhang G, Wu Y, Wang W, Zeng W, Ding M, Cui J, Wu Z, Wang LY,
569 Ding J (2016) Extrapolating microdomain Ca(2+) dynamics using BK channels as a Ca(2+)
570 sensor. Sci Rep 6:17343.
571 Hu H, Gan J, Jonas P (2014) Interneurons. Fast-spiking, parvalbumin(+) GABAergic interneurons:
572 from cellular design to microcircuit function. Science 345:1255263.
573 Janickova L, Rechberger KF, Wey L, Schwaller B (2020) Absence of parvalbumin increases
574 mitochondria volume and branching of dendrites in inhibitory Pvalb neurons in vivo: a
575 point of convergence of autism spectrum disorder (ASD) risk gene phenotypes. Mol
576 Autism 11:47.

577 Jedrzejewska-Szmek J, Dorman DB, Blackwell KT (2023) Making time and space for calcium control
578 of neuron activity. Curr Opin Neurobiol 83:102804.
579 Jung S, Chung Y, Lee Y, Lee Y, Cho JW, Shin EJ, Kim HC, Oh YJ (2019) Buffering of cytosolic calcium
580 plays a neuroprotective role by preserving the autophagy-lysosome pathway during
581 MPP(+)-induced neuronal death. Cell Death Discov 5:130.
582 Kumar P, Goettemoeller AM, Espinosa-Garcia C, Tobin BR, Tfaily A, Nelson RS, Natu A, Dammer
583 EB, Santiago JV, Malepati S, Cheng L, Xiao H, Duong DD, Seyfried NT, Wood LB, Rowan
584 MJM, Rangaraju S (2024) Native-state proteomics of Parvalbumin interneurons identifies
585 unique molecular signatures and vulnerabilities to early Alzheimer's pathology. Nat
586 Commun 15:2823.
587 Leblond CS et al. (2014) Meta-analysis of SHANK Mutations in Autism Spectrum Disorders: a
588 gradient of severity in cognitive impairments. PLoS Genet 10:e1004580.
589 Leybaert L, Sanderson MJ (2012) INTERCELLULAR Ca
590 WAVES: MECHANISMS AND FUNCTION. Physiol Rev 92:1359-1392.
591 Ma X, Miraucourt LS, Qiu H, Sharif-Naeini R, Khadra A (2023) Modulation of SK Channels via
592 Calcium Buffering Tunes Intrinsic Excitability of Parvalbumin Interneurons in Neuropathic
593 Pain: A Computational and Experimental Investigation. J Neurosci 43:5608-5622.
594 Maravall M, Mainen ZF, Sabatini BL, Svoboda K (2000) Estimating intracellular calcium
595 concentrations and buffering without wavelength ratioing. Biophys J 78:2655-2667.
596 Matthews EA, Dietrich D (2015) Buffer mobility and the regulation of neuronal calcium domains.
597 Front Cell Neurosci 9:48.
598 Morales M, Margolis EB (2017) Ventral tegmental area: cellular heterogeneity, connectivity and
599 behaviour. Nat Rev Neurosci 18:73-85.
600 Nanou E, Catterall WA (2018) Calcium Channels, Synaptic Plasticity, and Neuropsychiatric Disease.
601 Neuron 98:466-481.
602 Pchitskaya E, Popugaeva E, Bezprozvanny I (2018) Calcium signaling and molecular mechanisms
603 underlying neurodegenerative diseases. Cell Calcium 70:87-94.
604 Peca J, Feliciano C, Ting JT, Wang W, Wells MF, Venkatraman TN, Lascola CD, Fu Z, Feng G (2011)
605 Shank3 mutant mice display autistic-like behaviours and striatal dysfunction. Nature
606 472:437-442.

Ruden JB, Dugan LL, Konradi C (2021) Parvalbumin interneuron vulnerability and brain disorders. Neuropsychopharmacology 46:279-287.

Santoro B, Shah MM (2020) Hyperpolarization-Activated Cyclic Nucleotide-Gated Channels as Drug Targets for Neurological Disorders. Annu Rev Pharmacol Toxicol 60:109-131.

Schultz W, Dayan P, Montague PR (1997) A neural substrate of prediction and reward. Science 275:1593-1599.

Schwaller B (2020) Cytosolic Ca(2+) Buffers Are Inherently Ca(2+) Signal Modulators. Cold Spring Harb Perspect Biol 12.

Tang X, Jaenisch R, Sur M (2021) The role of GABAergic signalling in neurodevelopmental disorders. Nat Rev Neurosci 22:290-307.

Wang X, Xu Q, Bey AL, Lee Y, Jiang YH (2014) Transcriptional and functional complexity of Shank3 provides a molecular framework to understand the phenotypic heterogeneity of SHANK3 causing autism and Shank3 mutant mice. Mol Autism 5:30.

Wang X et al. (2016) Altered mGluR5-Homer scaffolds and corticostriatal connectivity in a Shank3 complete knockout model of autism. Nat Commun 7:11459.

Yi F, Danko T, Botelho SC, Patzke C, Pak C, Wernig M, Sudhof TC (2016) Autism-associated SHANK3 haploinsufficiency causes Ih channelopathy in human neurons. Science 352:aaf2669.

Zhou Z, Neher E (1993) Mobile and immobile calcium buffers in bovine adrenal chromaffin cells. J Physiol 469:245-273.

Zhu M, Idikuda VK, Wang J, Wei F, Kumar V, Shah N, Waite CB, Liu Q, Zhou L (2018) Shank3-deficient thalamocortical neurons show HCN channelopathy and alterations in intrinsic electrical properties. J Physiol 596:1259-1276.

Figures and Tables

Figure 1. Abnormal action potential (AP) firing and resting membrane potential (RMP) in Shank3-/- VTA DA neurons.

A. Left, distribution of DA neurons in the whole brain. Red, immunostaining of tyrosine hydroxylase (TH) as a marker for DA neurons; blue, DAPI as a marker for cell nuclei. Scale bar, 1 mm. Right, three types of VTA DA neurons filled with AF594 as a tracer for cell morphology. Scale bar, 20 mm.

B. AP firing of VTA DA neurons from WT and Shank3-/- mice evoked by current injection (150 pA).

C. Averaged results show reduced AP firing in Shank3-/- neurons. Animals used: 4 (WT), 3 (Shanl3-/-). Neurons recorded, 12 (WT), 14 (Shank3-/-). P-value: 50 pA, 0.002; 75 pA, 0.010.

D. AP half-width vs. current injection amplitude. Black, WT (n=14); Red, Shank3-/- (n=24). Neurons recorded, 12 (WT), 9 (Shank3-/-). P-value: 200 pA, 0.024.

E. AP amplitude vs. current injection amplitude. Black, WT (n=14); Red, Shank3-/- (n=24). Neurons recorded, 13 (WT), 14 (Shank3-/-). P-value: 200 pA, 0.008.

F. Averaged RMP and Rin of WT and Shank3-/- DA neurons. Animals used: 7 (WT), 10 (Shanl3-/-). Neurons recorded, 14 (WT), 24 (Shank3-/-). P-value: RMP, 0.020; Rin, 0.901.

Figure 2. Abnormal calcium transients in the soma of Shank3-/- VTA DA neurons.

A. Two-photon imaging of somatic calcium transients in WT (left) and Shank3-/- (right) DA neurons. 4 current pulse injections, with the setting of 2 nA / 2 msec / 2 Hz, were used to elicit AP firing. Top, current pulse. Bottom, membrane potential.

B. Calcium transients recorded with 200 mM Fluo-4 (K_D, 345 nM) added to the pipette solution.

C. Overlay of WT (black) and Shank3-/- (red) calcium transients recorded with 200 mM Fluo-4 loaded through the whole-cell recording electrode.

D. Overlay of WT (black) and Shank3-/- (red) calcium transients recorded with 250 mM Fluo-5F.

E. Averaged results of the decay time constant (left) and the amplitude of the four calcium peaks (right). Measured with Fluo-4 in the pipette solution. Animals used: 2 (WT), 2 (Shanl3-/-). Neurons recorded, 7 (WT), 7 (Shank3-/-). P-value: tau, 0.013; DF/F (peaks 1-4), 0.057, 0.072, 0.143, 0.138.

F. Averaged results of the decay time constant (left) and the amplitude of the four calcium peaks (right). Measured with Fluo-5F in the pipette solution. Animals used: 5 (WT), 5 (Shanl3-/-). Neurons recorded, 7 (WT), 9 (Shank3-/-). P-value: tau, 0.012; DF/F (peaks 1-4), 0.179, 0.336, 0.296, 0.648.

Figure 3. Altered calcium transient profile in Shank3-/- VTA DA neuron dendric shaft.

A. Left, two-photon fluorescence image of a VTA DA neuron filled with AF594 (red channel) and Fluo-4. Right, calcium transients evoked by a train of 4 current pulses (2 nA, 2 msec, 2 Hz). Overlay of calcium transient traces recorded from dendrites (50, 100, 150 mm from soma; top to bottom) from WT and Shank3-/- DA neurons (WT, n=7; Shank3-/-, n=7; right).

B. Averaged results of the decay time constant of dendritic calcium transients as a function of distance from the soma. Animals used: 2 (WT), 2 (Shanl3-/-). Neurons recorded, 10 (WT), 15 (Shank3-/-). P-value: tau (50-100-150), 0.003, 0.014, 0.001.

C. Statistics of 4 peaks of calcium transients recorded from three dendritic locations. P-value: (50 – 100 – 150 mm) peak 1, 0.0002 0.0004 0.008; peak 2, 0.005 0.012 0.011; peak 3, 0.002 0.018 0.046; peak 4 0.031 0.019 0.009.

D. Left, two-photon fluorescence image of a VTA DA neuron filled with AF594 (red channel) and Fluo-5F. Right, calcium transients evoked by a train of 4 current pulses (2 nA, 2 msec, 2 Hz). Overlay of calcium transient traces recorded from dendrites (50, 100, 150 mm from soma; top to bottom) from WT and Shank3-/- DA neurons (WT, n=8; Shank3-/-, n=10; right).

E. Averaged results of the decay time constant of dendritic calcium transients. Animals used: 4(WT), 5 (Shanl3-/-). Neurons recorded, 11 (WT), 10 (Shank3-/-). P-value: tau (50-100-150), 0.013, 0.037, 0.030.

F. Statistics of 4 peaks of calcium transients recorded from three dendritic locations. P-value: (50 – 100 – 150 mm) peak 1, 0.015 0.018 0.050; peak 2, 0.048 0.147 0.522; peak 3, 0.058 0.077 0.311; peak 4 0.277 0.241 0.993.

Figure 4. Mass-spectrometry revealed a reduced level of PV protein in Shank3-/- VTA area.

A. Schematic illustration of the mass spectrometry analysis of isolated brain tissues from WT (n=3) and Shank3-/- (n=3) VTA regions. A total of 4882 proteins were identified, with 132 proteins showing differential expression between WT and SHANK3-/- samples ($P < 0.05$).

B. Volcano plot of mass spectrometry results showing proteins with significantly upregulated levels (right, red, 86) and down-regulated levels (left, green, 46). The X- and Y-axis represent the fold change in log2 and the logarithm of the P-value, respectively.

C. Gene-ontology (GO) analysis results are categorized into biological processes (BP, green), cellular components (CC, orange), and molecular functions (MF, blue). The X-axis indicates the number of proteins in each significantly enriched term (p-adjust < 0.05).

D. Statistics of KEGG enrichment of WT and Shank3-/- results, including 10 significantly enriched pathways (Y-axis, p-adjust < 0.05) and 21 genes (X-axis). Bubble color represents the $\log_2$ fold change (FC) value of each gene, with orange denoting up-regulated and green indicating down-regulated expression in the Shank3 −/− group relative to WT.

E. Immunostaining of PV (green) and TH (red) in coronal slices of WT and Shank3-/- brains. Collected by 10X lens and assembled by Image Mosaicing program. Scale bar, 1 mm.

F. PV expression in the VTA area of WT and Shank3-/- mice. Collected by 60X oil lens. Scale bar, 50 mm.

G. Zoomed-in view over the box shown in G. Notice that the much weaker green signal (PV) in Shank3-/- neurons makes the composite image appear red, in contrast to the yellowish image of WT neurons.

H. Statistics of immunostaining results. Animals used: 3 (WT), 4 (Shank3-/-). Brain slices imaged, 10 (WT), 12 (Shank3-/-). P-value, neuron number 0.212, TH 0.042, PV, <0.0001.

Figure 5. Quantification of somatic calcium buffer capacity in WT and Shank3-/- VTA DA neurons by Fluo-4 two-photon imaging.

A. Representative IR-DIC image of a VTA DA neuron and the corresponding two-photon images of the soma (with recording electrode) filled with AF594 (10 μM) and Fluo-4 (200 μM). Somatic calcium transients elicited by 4 current injections (2 msec, 2 Hz, 2 nA). Top, current injections; bottom, membrane potential signal.

B. Normalized calcium transients recorded at two time points.

C. Fluorescence intensity (black) and K_B (red) as a function of time after seal rupture and the formation of whole-cell recording configuration.

D. Time constant of the decay of calcium transients as a function of recording time.

E. Cross plot of time constant and K_B and the linear regression fit.

F. Statistics of the K_E values of WT (black) and Shank3-/- (red) neurons. Animals used: 3 (WT), 5 (Shank3-/-). Neurons recorded, 7 (WT), 7 (Shank3-/-). P-value: 0.033.

G. Equations for the calculation of K_B and t-K_B-K_E relationship.

Figure 6. Quantification of somatic calcium buffer capacity in WT and Shank3-/- VTA DA neurons by Fura-8 ratiometric calcium imaging.

A. Configuration of the home-built imaging system for ratiometric calcium measurements.

B. Raw images of a WT VTA DA neuron filled with 50 mM Fura-8 and recorded at three different time points as indicated by * in the figure below. Top, 365 nm excitation; bottom, 410 excitation. Scale bar, 20 mm.

C. DA neurons stimulated by a train of 16 current injections (2 nA, 2 msec, 50 Hz). Top, current injections; bottom, membrane potential.

D. Fluorescence intensities recorded with the excitation of 365 nm (top) and 410 nm (bottom). Left, WT; right, Shank3-/-.

E. Traces of F_{365}/F_{410} based on recordings shown in L.

F. Calcium transients (F_{365}/F_{410}) recorded from a WT DA neuron filled with 50 mM Fura-8 recorded at 4 min (top) and 16 min (bottom) after membrane break-in.

G. Fluorescence intensity and K_B as a function of time after membrane break-in.

H. Statistics of measured endogenous calcium buffer power (K_E) of WT (n=15) and Shank3-/- (n=15) VTA DA neurons. Animals used: 3 (WT), 3 (Shank3-/-). Neurons recorded, 10 (WT), 10 (Shank3-/-). P-value: <0.0001.

Figure 7. Schematic drawing shows Shank3 as a key structural protein in coordinating the protein surface expression and localization of numerous channels and receptors and the cytosolic expression of the PV protein.

Fig. 1

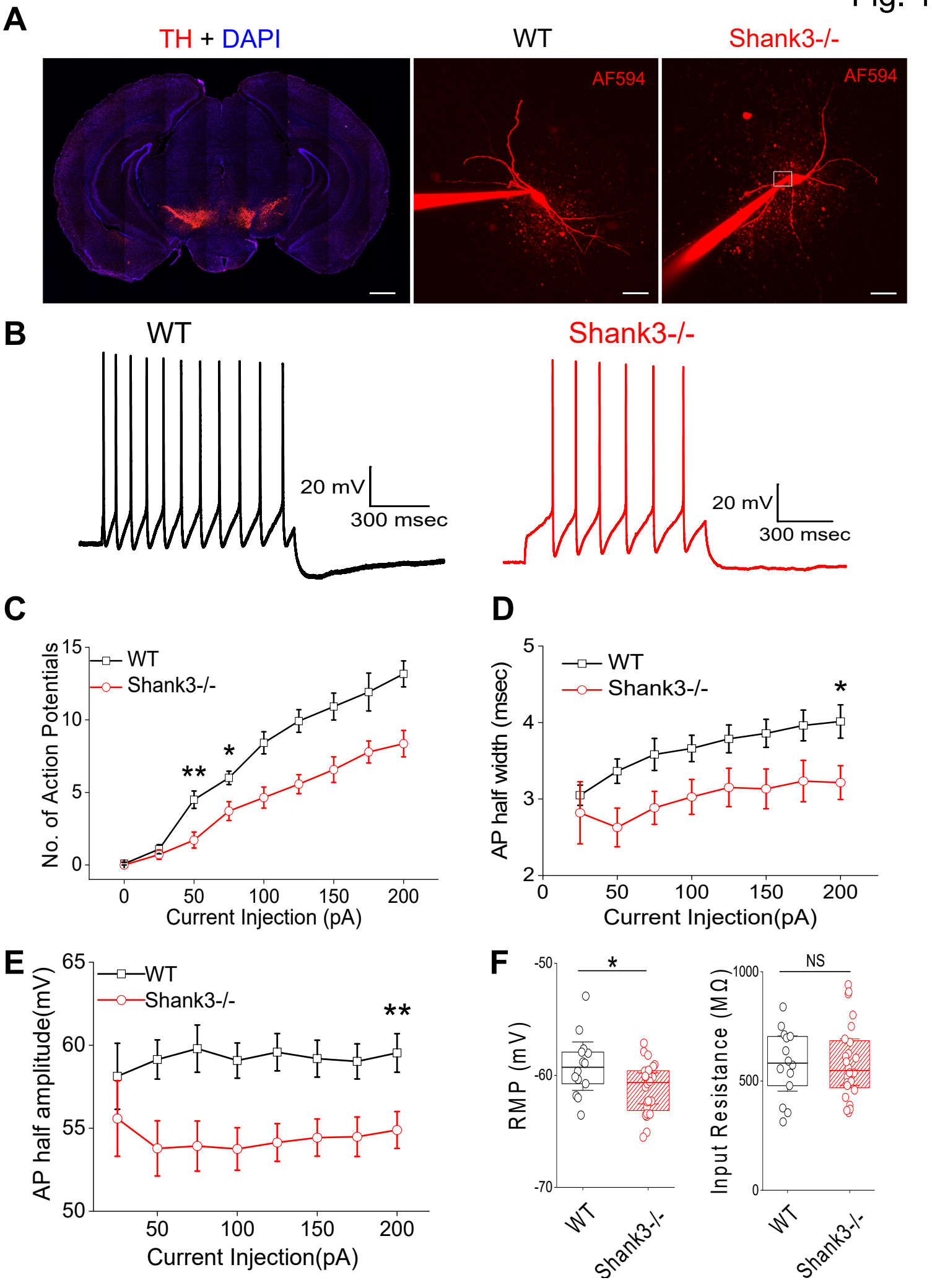

Fig. 2

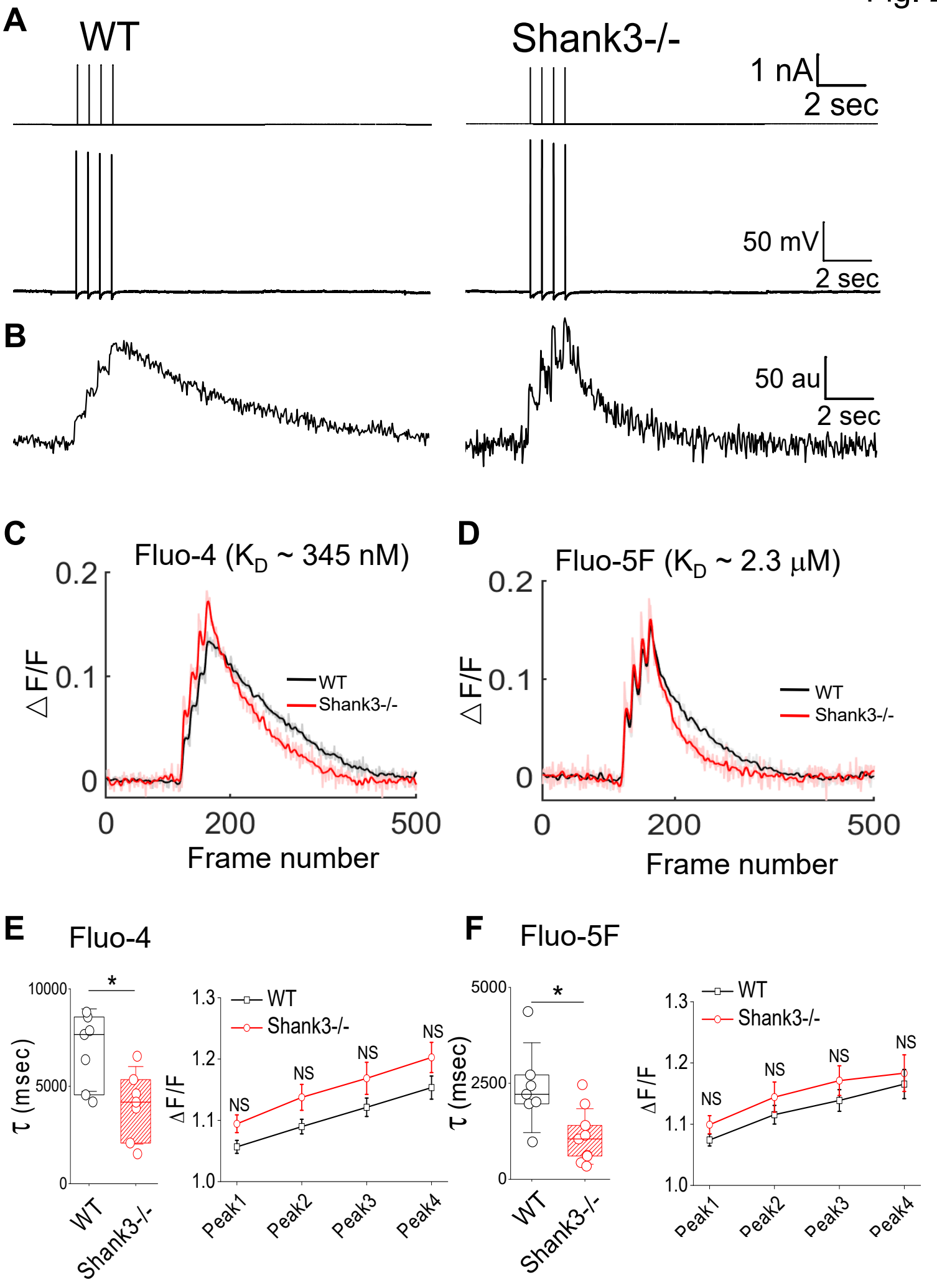

Fig. 3

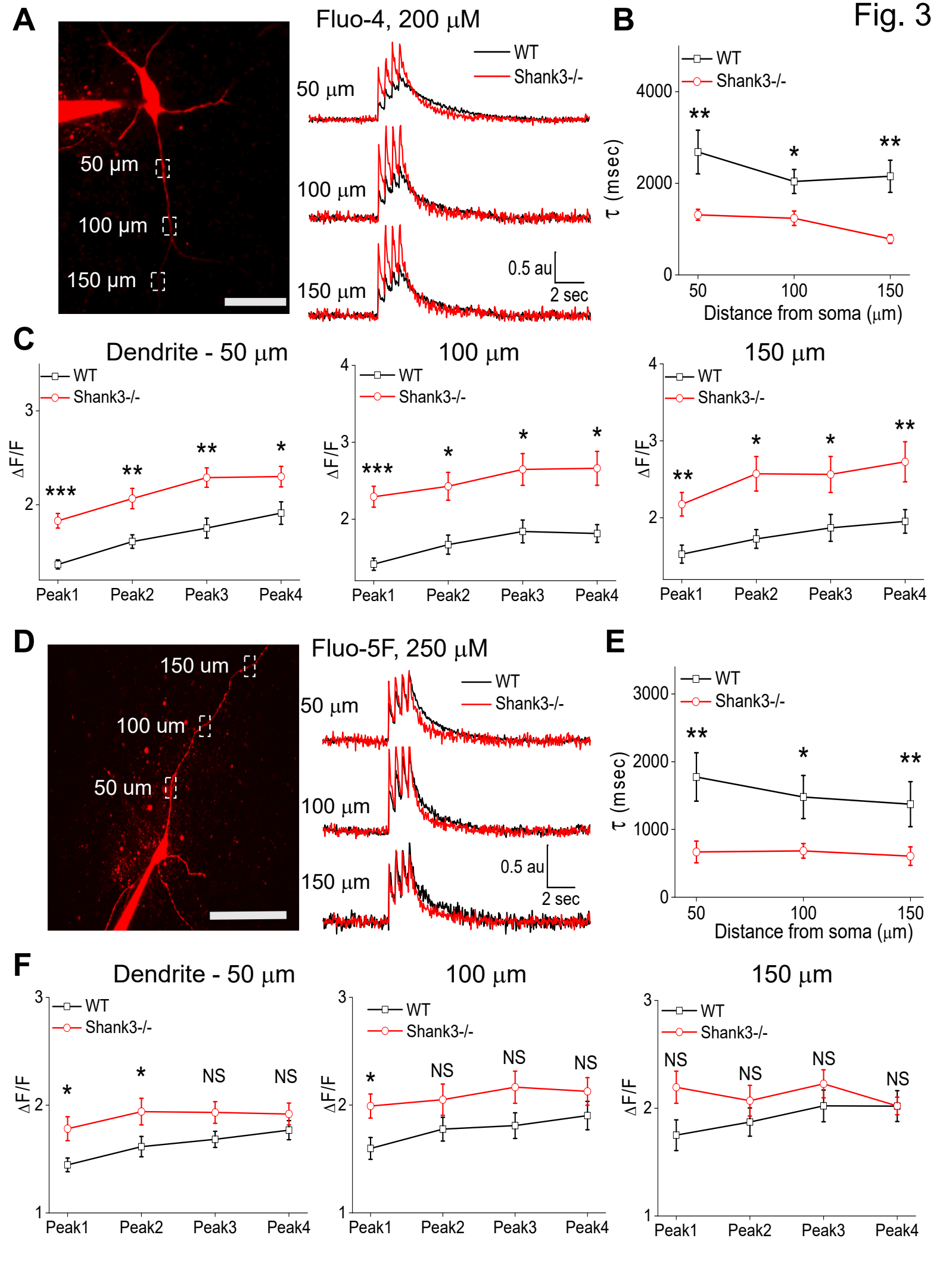

Fig. 4

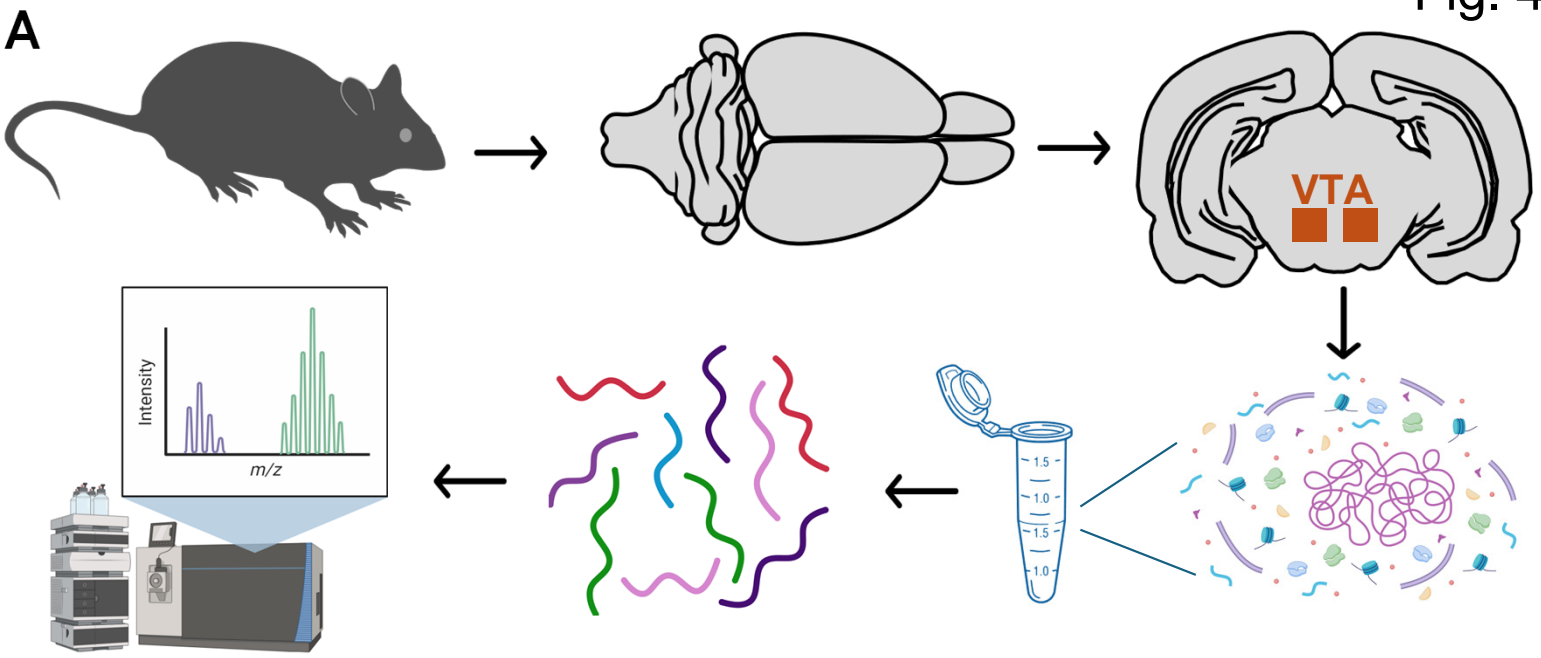

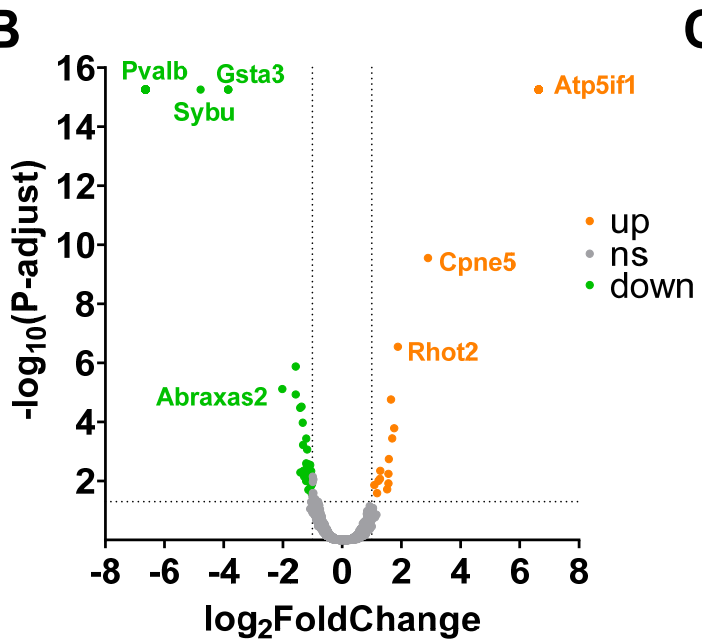

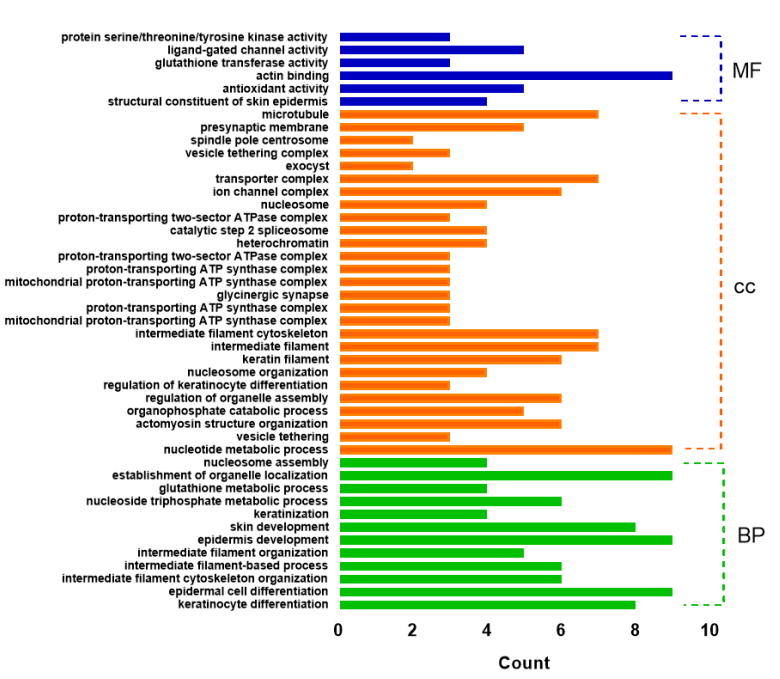

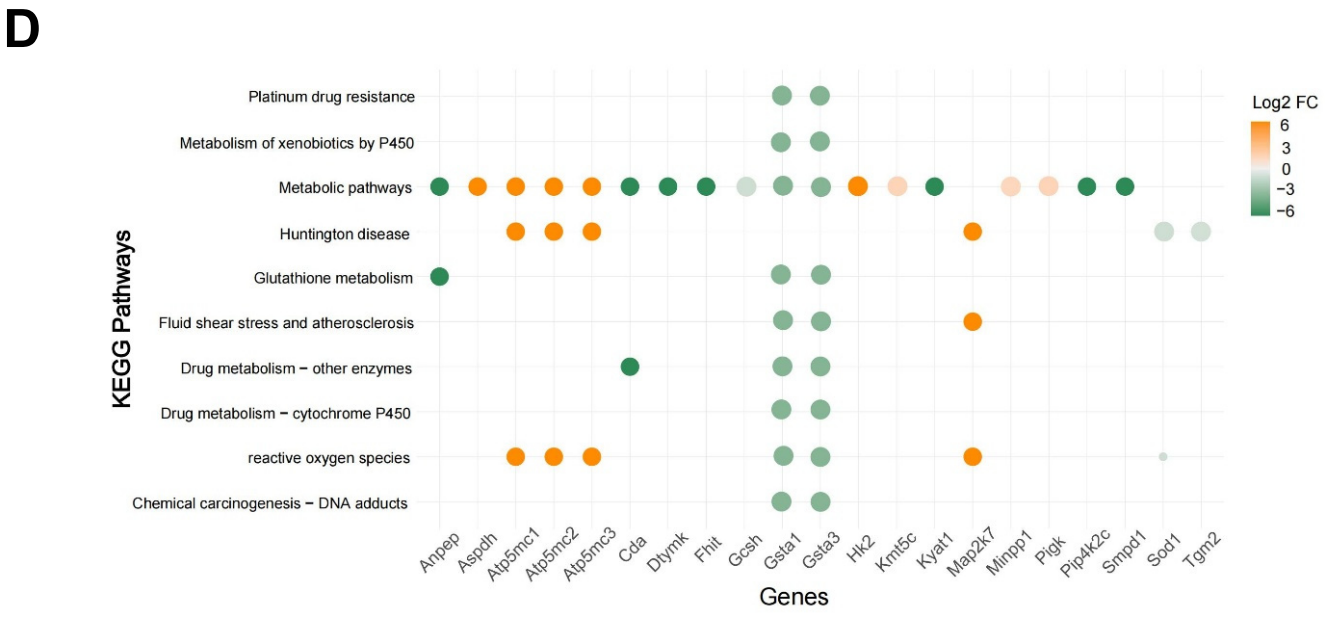

Fig. 4

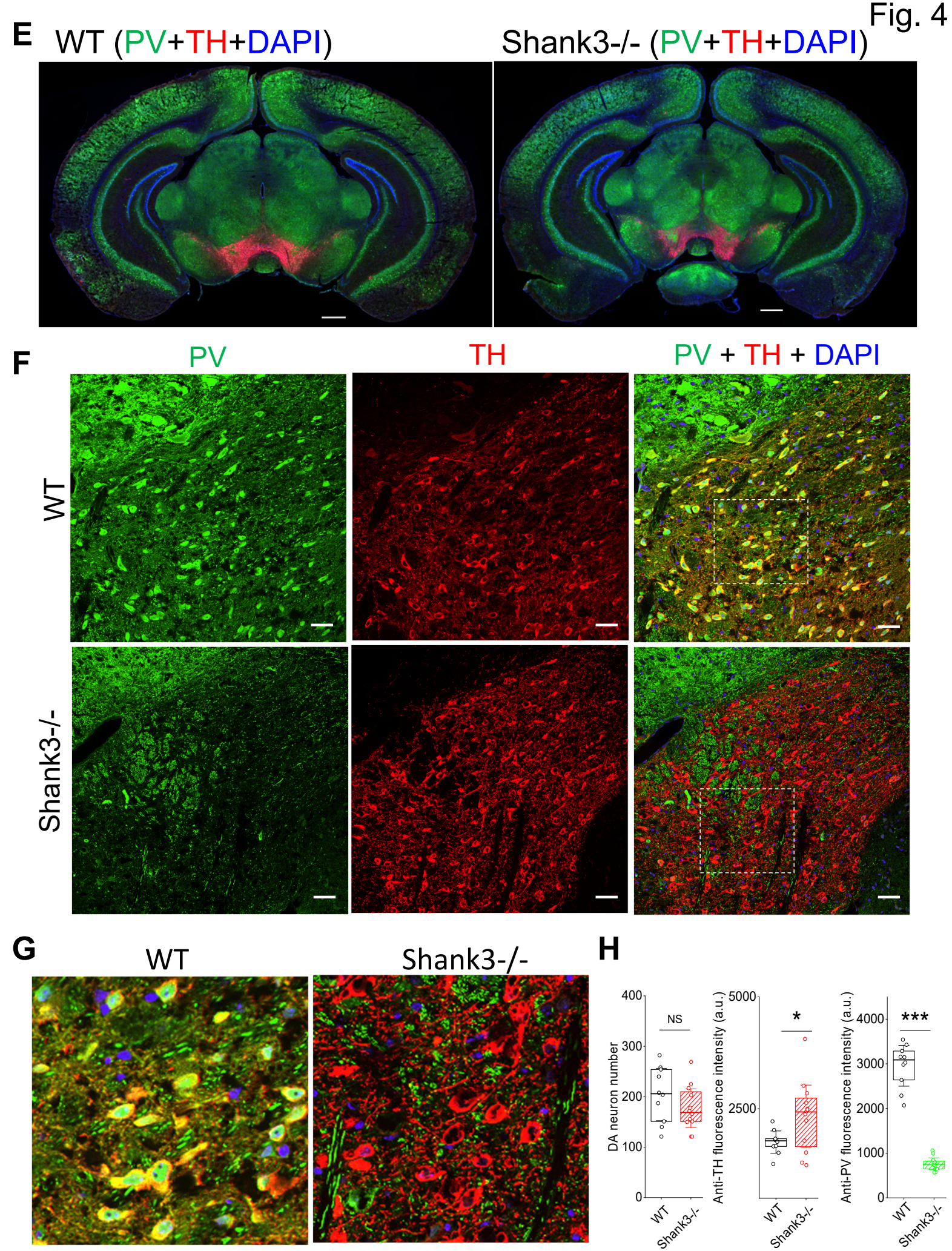

Fig. 5

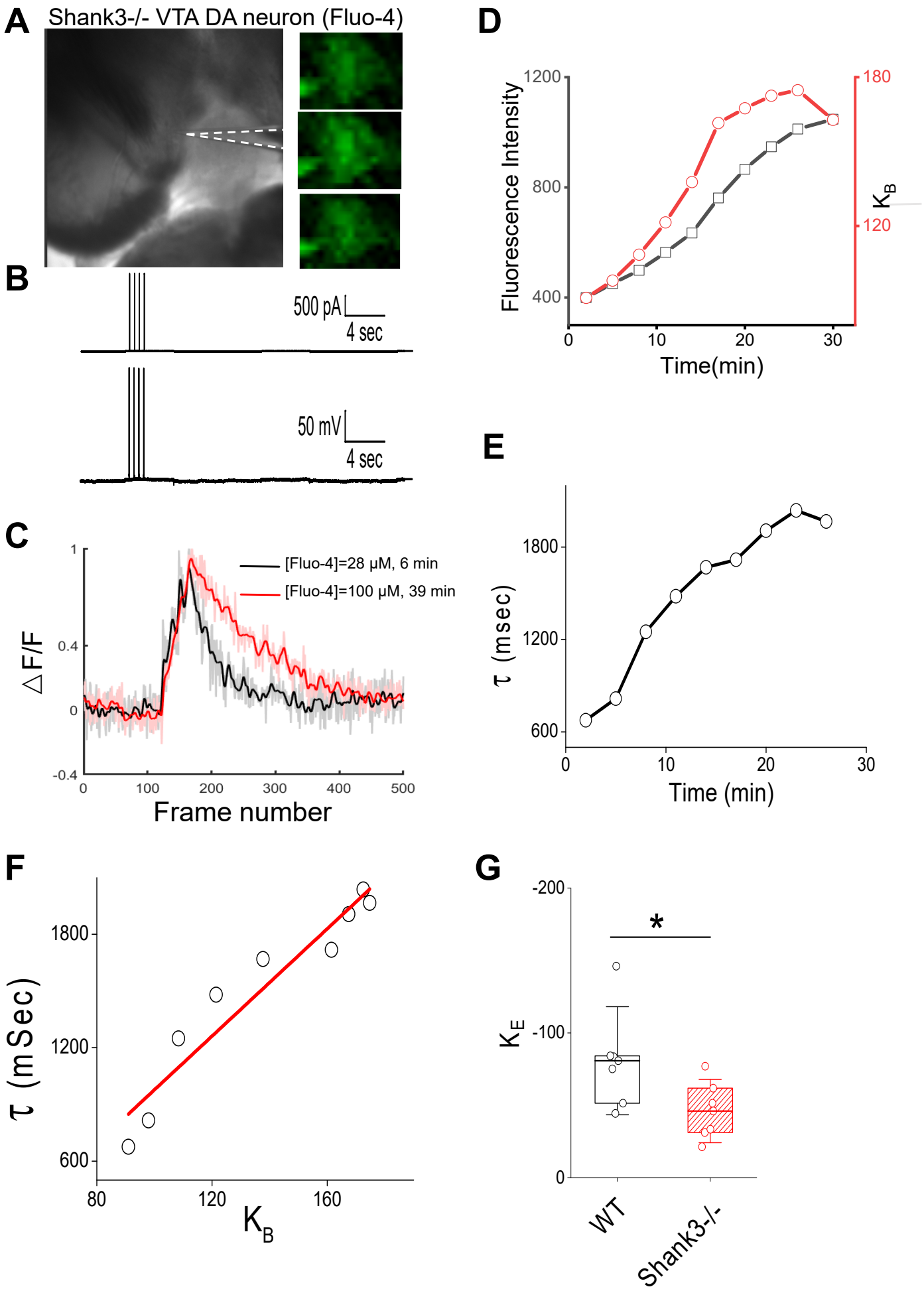

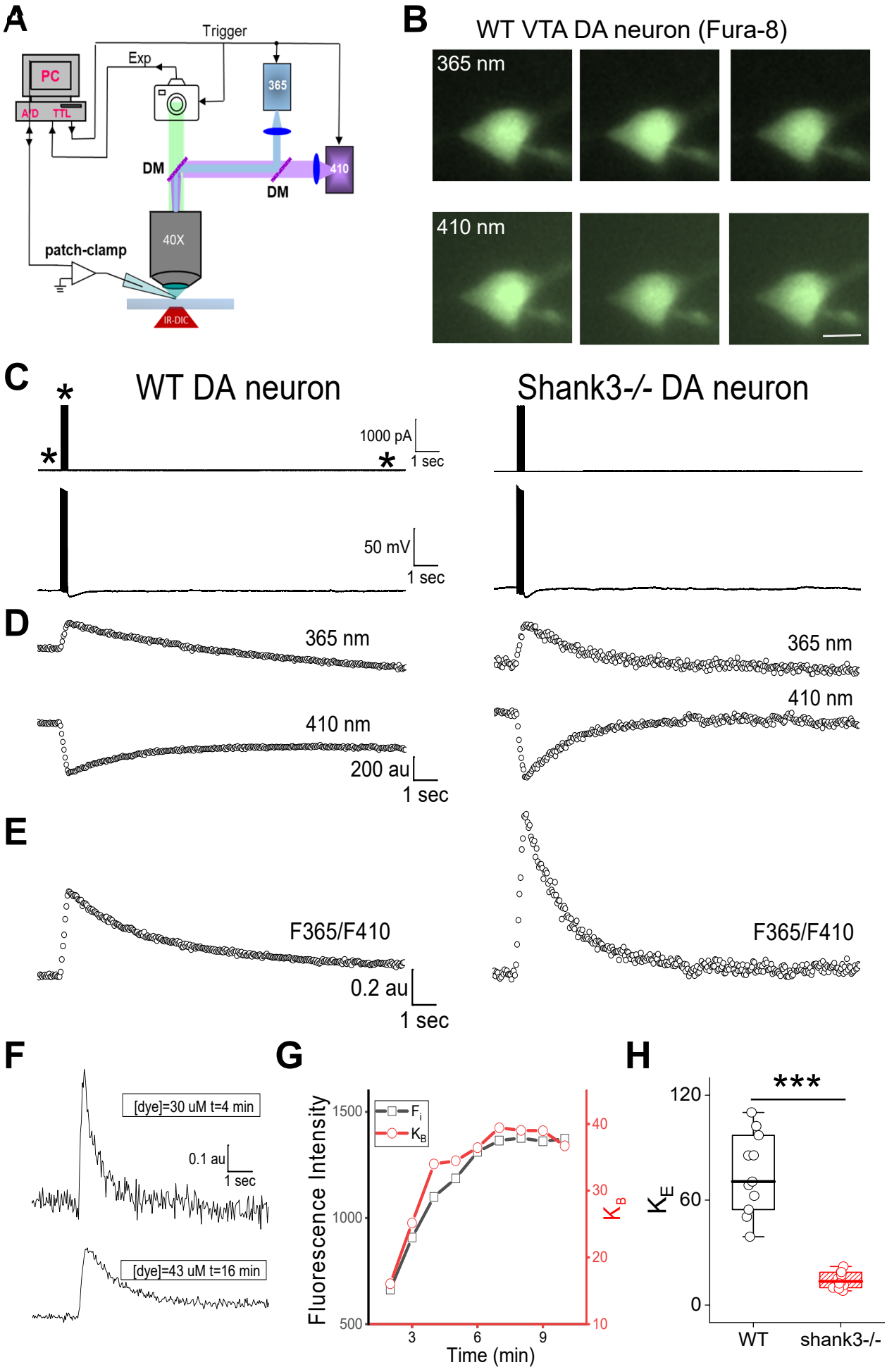

Fig. 7

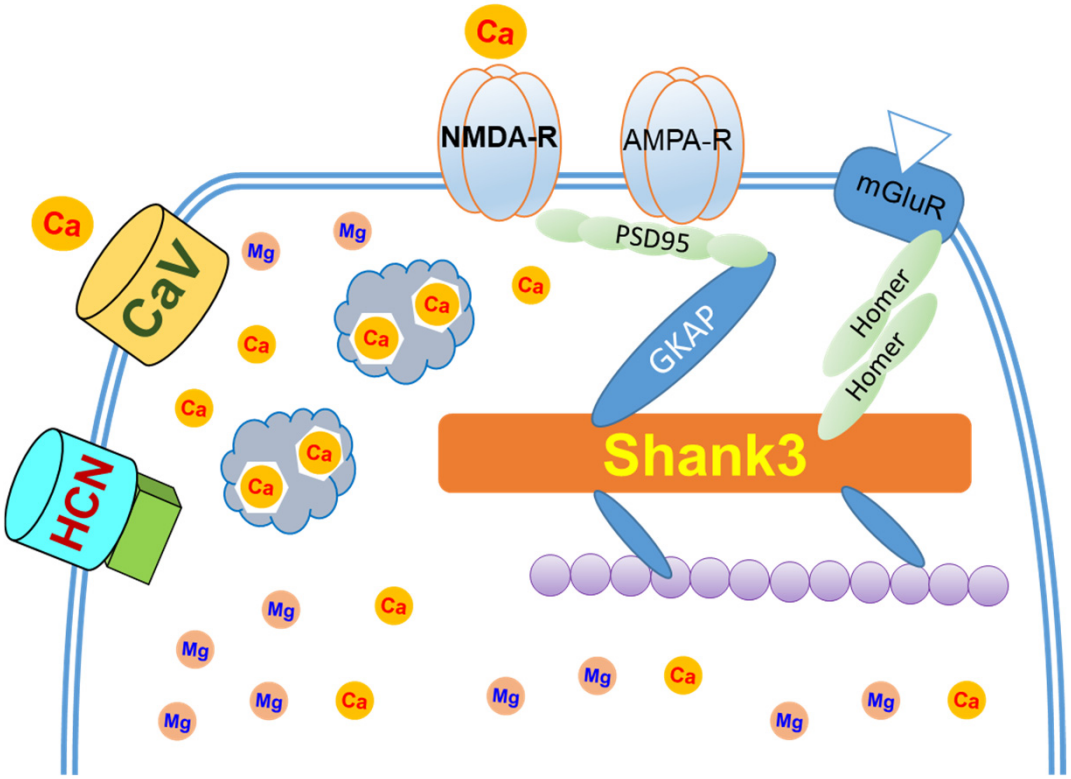

Supporting Information:

Fig. S1. Pharmacological perturbations of somatic calcium transients in WT VTA DA neurons.

A. Somatic calcium transients (bottom) evoked by four short current injections (2 nA, 2 msec, 50 Hz, top), recorded from a WT VTA DA neuron. The corresponding membrane potential is shown in the middle.

B. DHPG (50 mM, added in ACSF) prolonged the decay of the calcium transients shown in A.

C. Statistical results of the effect of DHPG on the decay time constant of calcium transients of WT (n=6, black, P-value, 0.017) and Shank3-/- (n=7, orange, P-value, <0.0001) VTA DA neurons.

D. Statistical results of the effect of caffeine (5 mM, added in ACSF) on the decay time constant of calcium transients of WT (n=8, black, P-value, <0.0001) and Shank3-/- (n=9, blue, P-value, <0.0001) VTA DA neurons.

E. Statistical results of the effect of ryanodine (75 mM, added in the pipette solution) on the decay time constant of calcium transients of WT (n=8, black, P-value, 0.271) and Shank3-/- (n=8, green, P-value, 0.701) VTA DA neurons.

F. Statistical results of the effect of isradipine (5 mM, added in ACSF) on the decay time constant of calcium transients of WT (n=9, black, P-value, 0.004) and Shank3-/- (n=9, red, P-value, 0.0014) VTA DA neurons. Type or paste legend here. Paste figure above the legend.

Fig. S2. Shank3 associated genes via PV identified by mass-spectrometry and protein-protein interaction (PPI).

Using the STRING database, PPI analysis of significantly differentially expressed genes reveals *Shank3* is associated with *Cbln1*, *Titin*, *TPM2*, *FLNC*, *FLNB*, and other genes via *PV*. Notably, *Cbln1* has been shown to rapidly induce synaptogenesis, while *TPM2* inhibits cell migration. Similarly, the significant downregulation of *SLIT2* may lead to increased cell migration. Downregulation of *FLNB* may result in reduced cell migration mediated by cell signaling perception, while significant downregulation of the *DYRK1A* gene and significant upregulation of the *DSCAM* gene both resulted in increased neuronal generation and maturation. Collectively, these results suggest that Shank3 deficiency may drive a cellular phenotype characterized by increased migration and impaired signaling centered on PV-associated pathways, potentially accompanied by impaired neuronal development and maturation.

Fig. S3. Reduced PV expression in Shank3-/- and Shank3+/- VTA DA neurons.

A. Immunostaining of PV (green), TH (red), and DAPI (blue) in coronal slices of WT and Shank3-/- mouse brain slices.

B. Statistics of immunostaining results. Total number of analyzed brain slices: 8 (WT), 9 (Shank3-/-). P-value: TH+ neuron number, 0.197; TH fluorescence, 0.218; PV fluorescence, <0.0001.

C. Immunostaining of PV (green), TH (red), and DAPI (blue) in WT and Shank3+/- mouse brain slices. Zoomed view of the regions indicated by dashed boxes are shown below.

D. Pixels with TH signal (red channel) higher than 50 are selected from the whole pictures shown in C, top. The corresponding PV signal intensities (green channel) of these pixels are pooled together and shown in histogram plots.

E. Left, histogram plots of 4 WT and 4 Shank3+/- brain slices support a significant decrease in PV expression in Shank3+/- VTA DA neurons. Right, statistical results of the PV signal intensities at peak distribution. Number of brain slices: 4; P-value, 0.0016.

F. *In-situ* hybridization (ISH) data of PV (left) and the corresponding reference brain atlas (right), obtained from websites of Allen Institute. A zoomed view of the VTA region is shown below.

Fig. S4. Immunostaining of PV in the cortex.

A. Immunostaining of PV (green) in coronal brain slices of WT (left) and Shank3-/- (right) mice. Scale bar, 100 mm.

B. Statistical results. Number of brain slices used in PV fluorescence analysis: WT, 9; Shank3-/-, 9. P-value: neuron number, 0.100; PV fluorescence, 0.001.

Fig. S5. Effects of adding additional EGTA in pipette solution on calcium transients recorded from VTA DA neurons.

A. Somatic calcium transients (bottom) elicited by four short current injections (2 nA, 2 msec, 2 Hz, top), recording from a Shank3-/- VTA DA neuron. The corresponding membrane potential is shown in the middle. Changes in neuronal calcium signaling induced by action potentials are shown in the bottom.

B. EGTA (350 mM, added in pipette solution) prolonged the decay of the calcium transients shown in A.

C. Image of a VTA DA neuron filled with AF594 and calcium indicator Fluo-5F.

D. The time constant of the decay of calcium transients recorded from the soma and three locations along the dendritic shaft. Black, control (Shank3-/-, n=8); red, Shank3-/- neurons filled with EGTA (n=8).

E. Amplitudes of 4 consecutive peaks of calcium signal recorded from the soma.

F. Amplitudes of 4 consecutive peaks of calcium signal recorded from three locations along the dendritic shaft (from left to right, 50, 100, and 150 mm from the soma).

Fig. S6. SDS-PAGE gel of protein samples collected during the expression and purification of recombinant PV protein.

Fig. S7. Effects of adding purified PV protein in pipette solution on calcium transients recorded from VTA DA neurons.

A. Somatic calcium transients (bottom) elicited by four short current injections (2 nA, 2 msec, 2 Hz, top), recorded from a Shank3-/- VTA DA neuron. The corresponding membrane potential is shown in the middle.

B. PV protein (5 mM, added in pipette solution) prolonged the decay of the calcium transients shown in A.

C. Image of a VTA DA neuron filled with AF594 and calcium indicator Fluo-5F.

D. The time constant of the decay of calcium transients recorded from the soma and three locations along the dendritic shaft. Black, control (Shank3-/-, n=8); red, Shank3-/- neurons filled with recombinant PV protein (n=9).

E. Amplitudes of 4 consecutive peaks of calcium transients recorded from the soma.

F. Amplitudes of 4 consecutive peaks of calcium transients recorded from three locations along the dendritic shaft (from left to right, 50, 100, and 150 mm from the soma).

Fig. S1

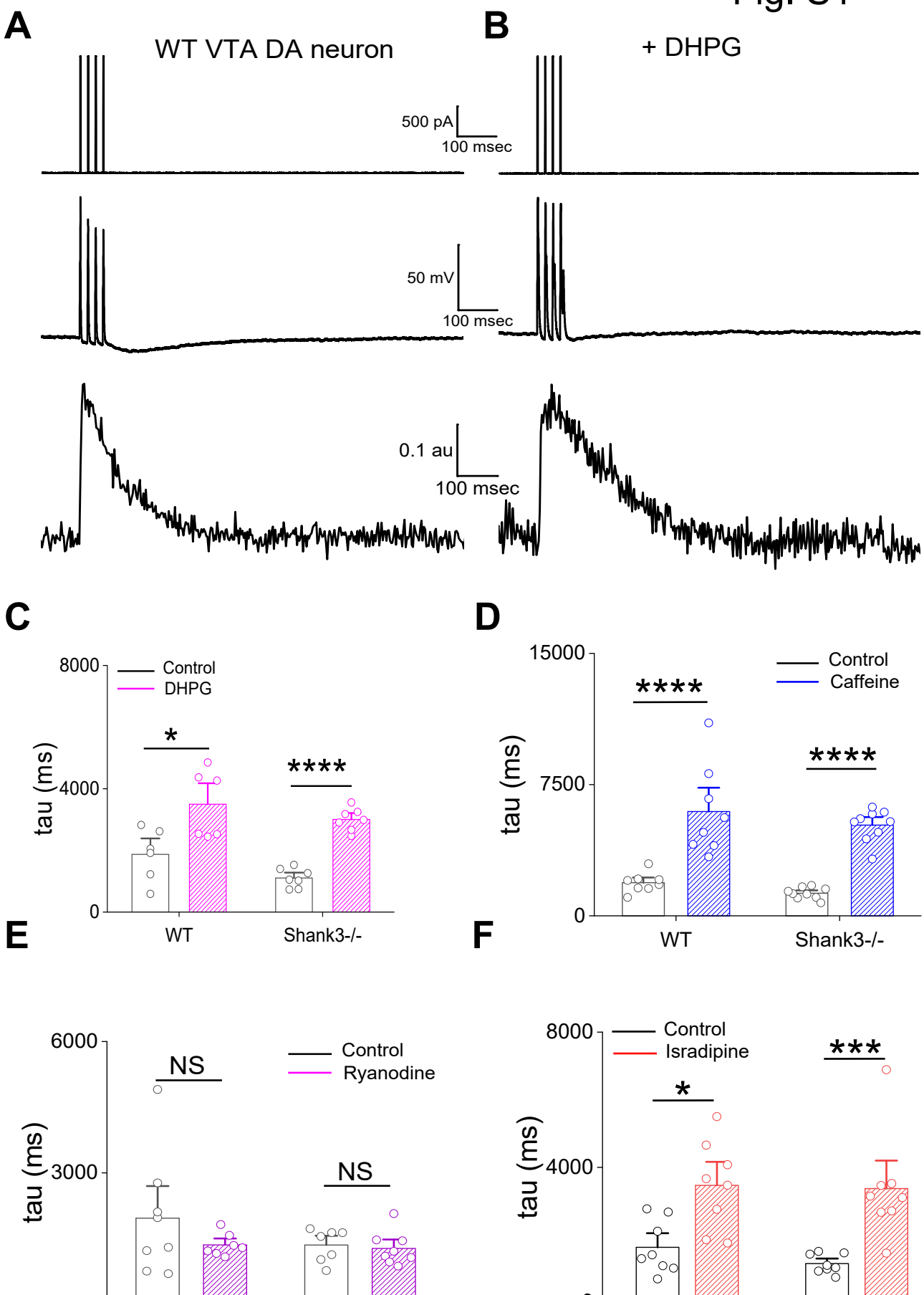

Fig. S2

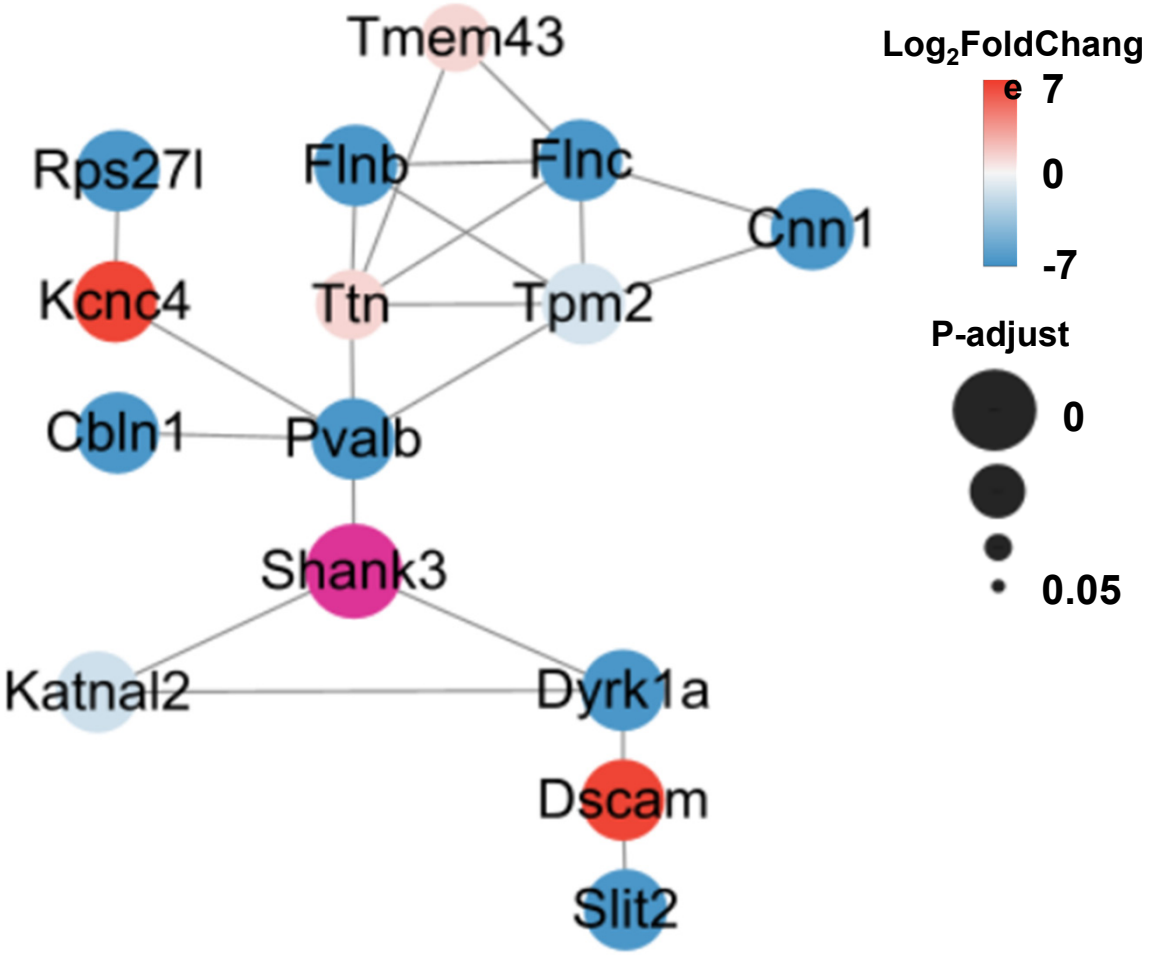

Fig. S3

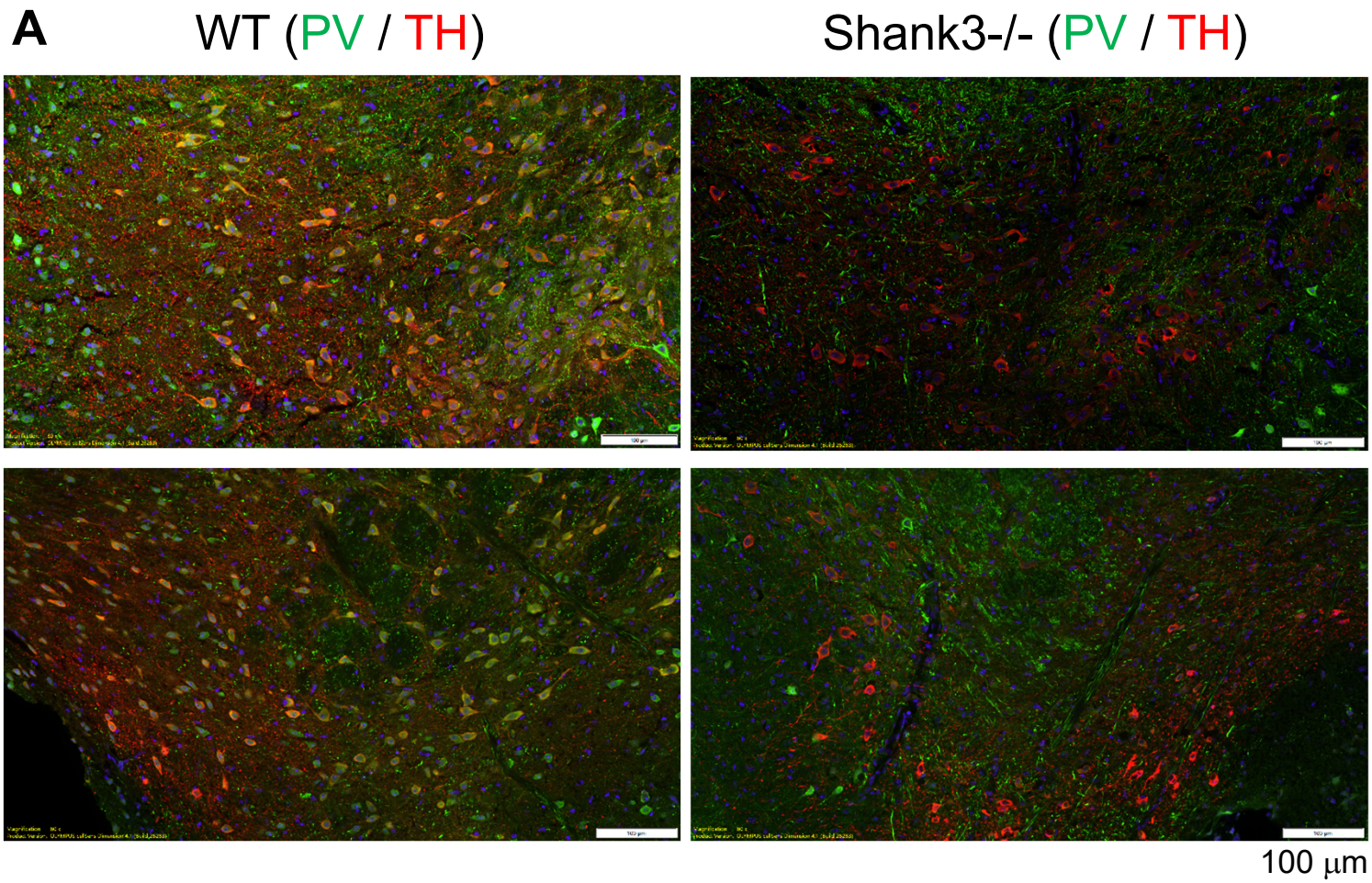

Fig. S3

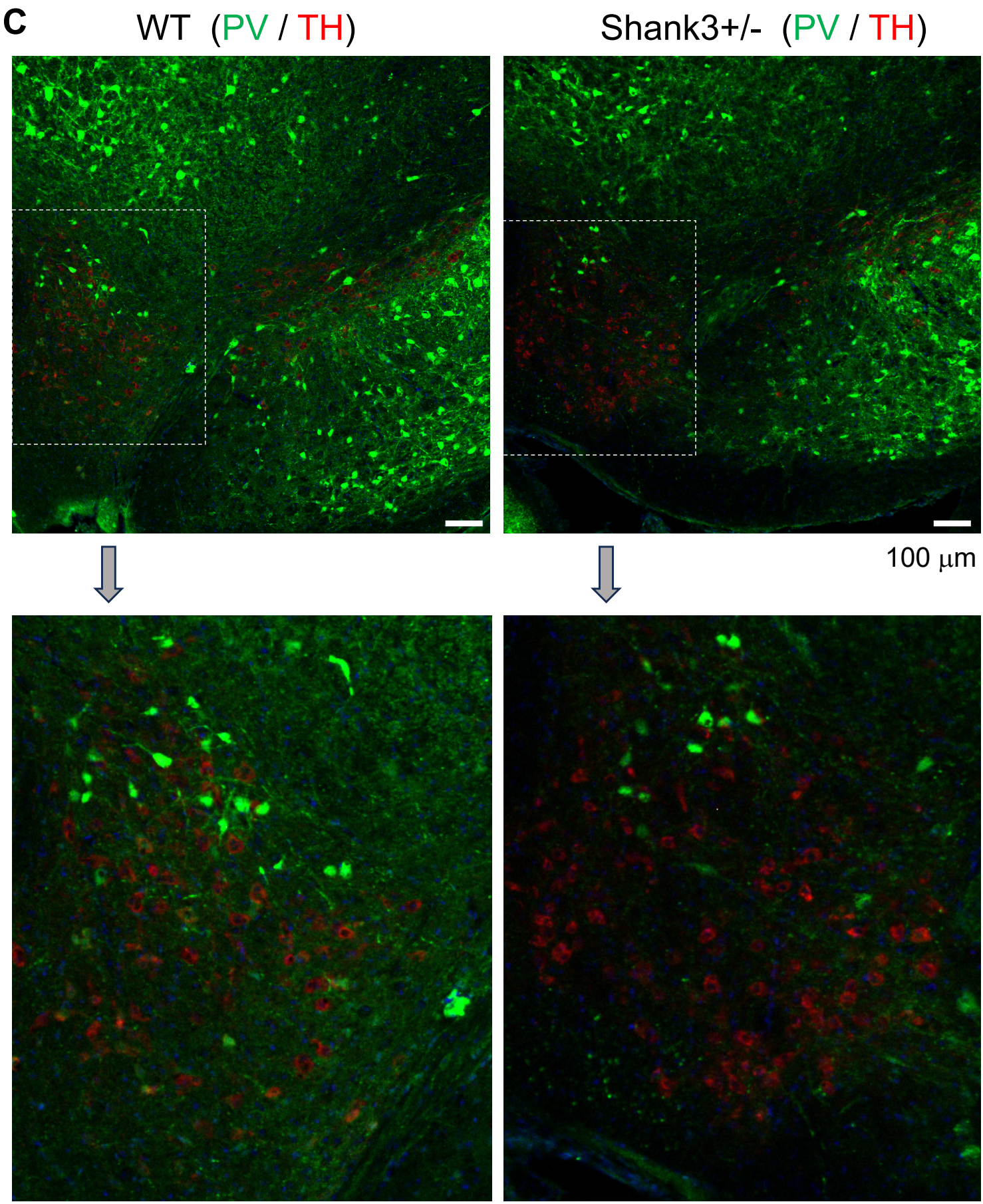

Fig. S3

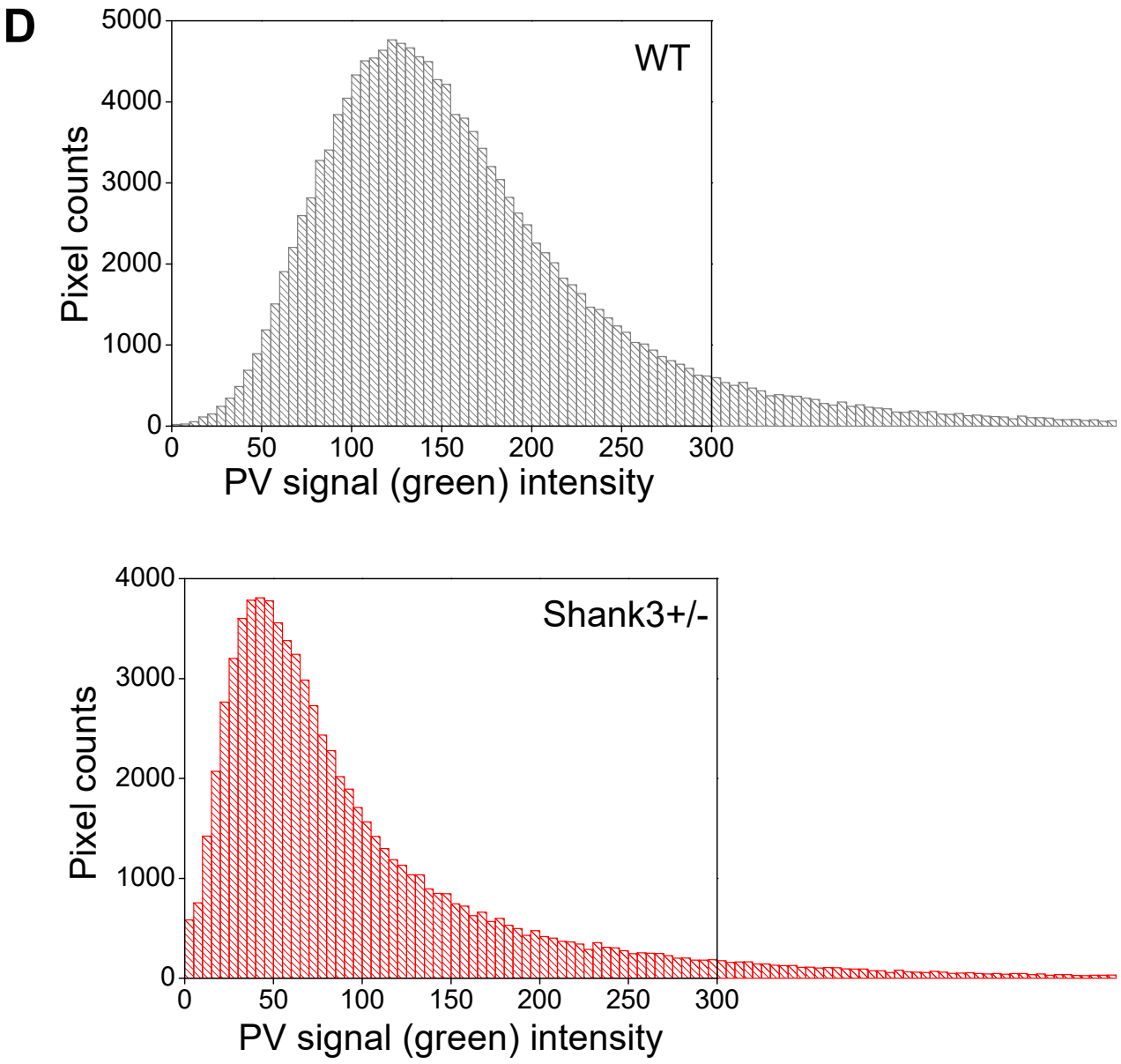

Fig. S3

F Parvalbumin *in situ* hybridization image data (Allen Institute; from https://atlas.brain-map.org/)

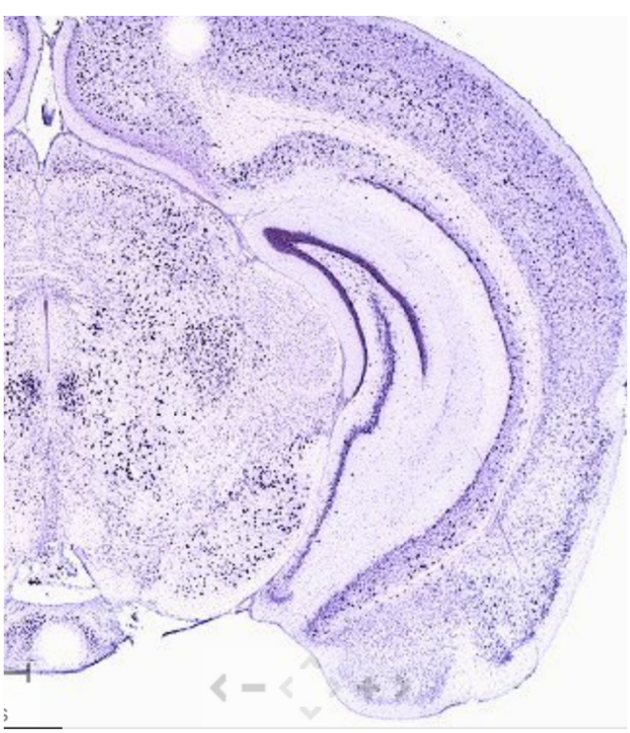

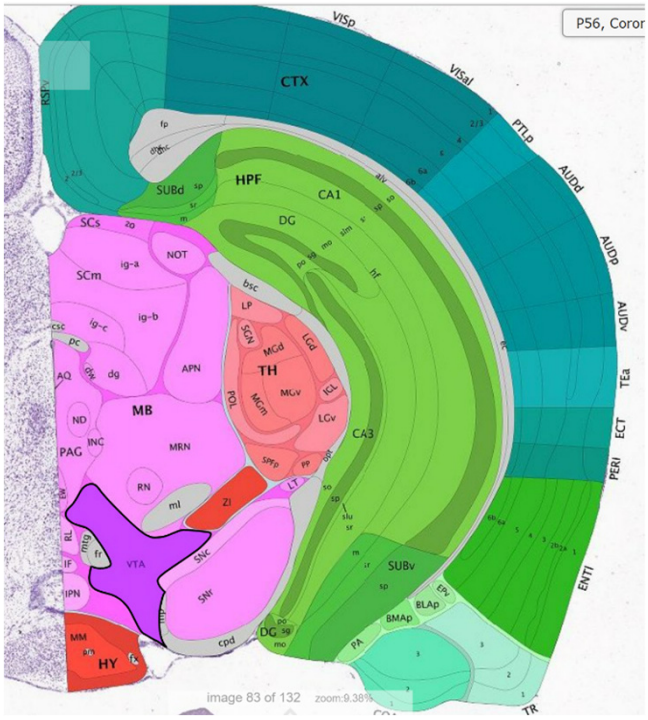

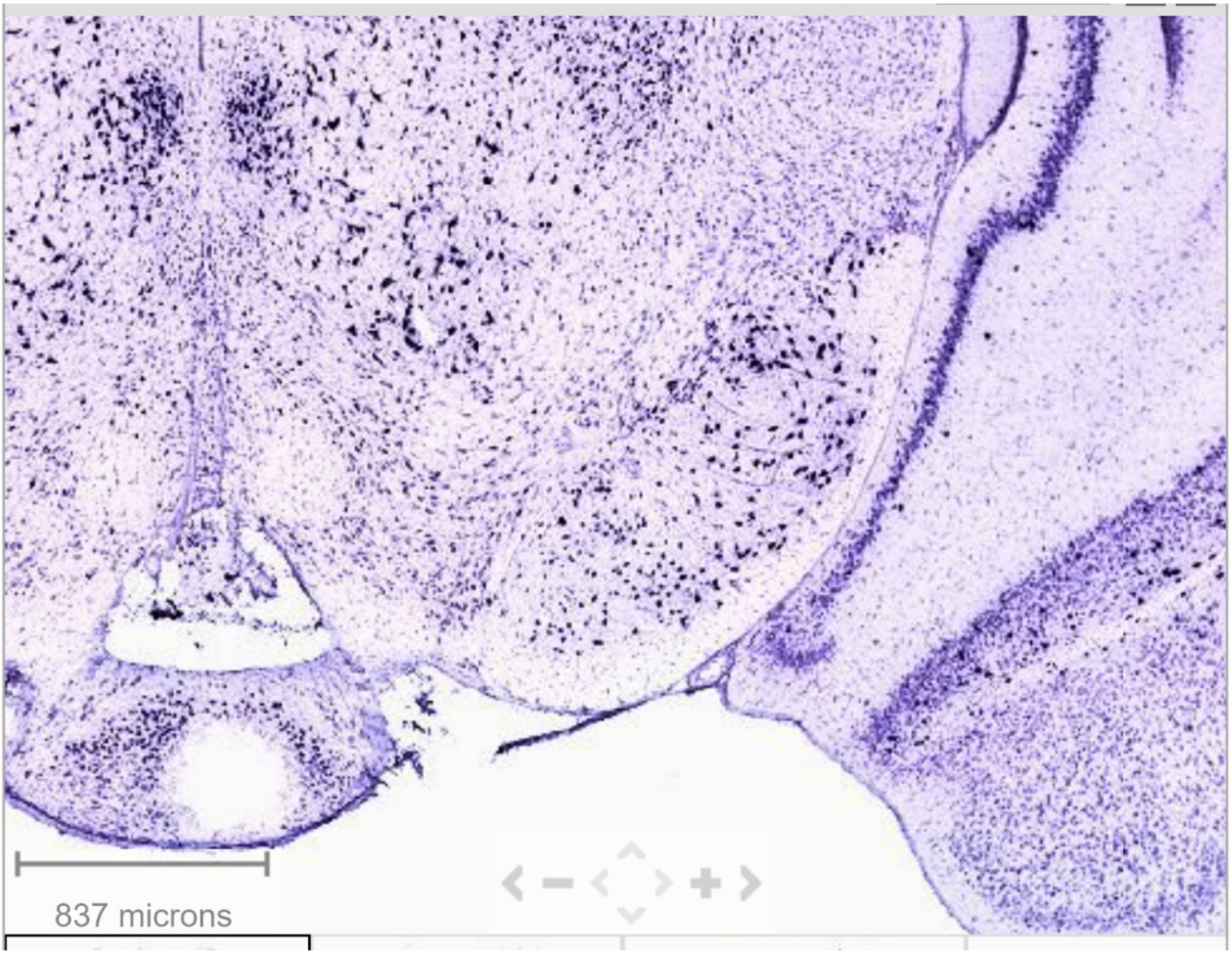

Fig. S4

A

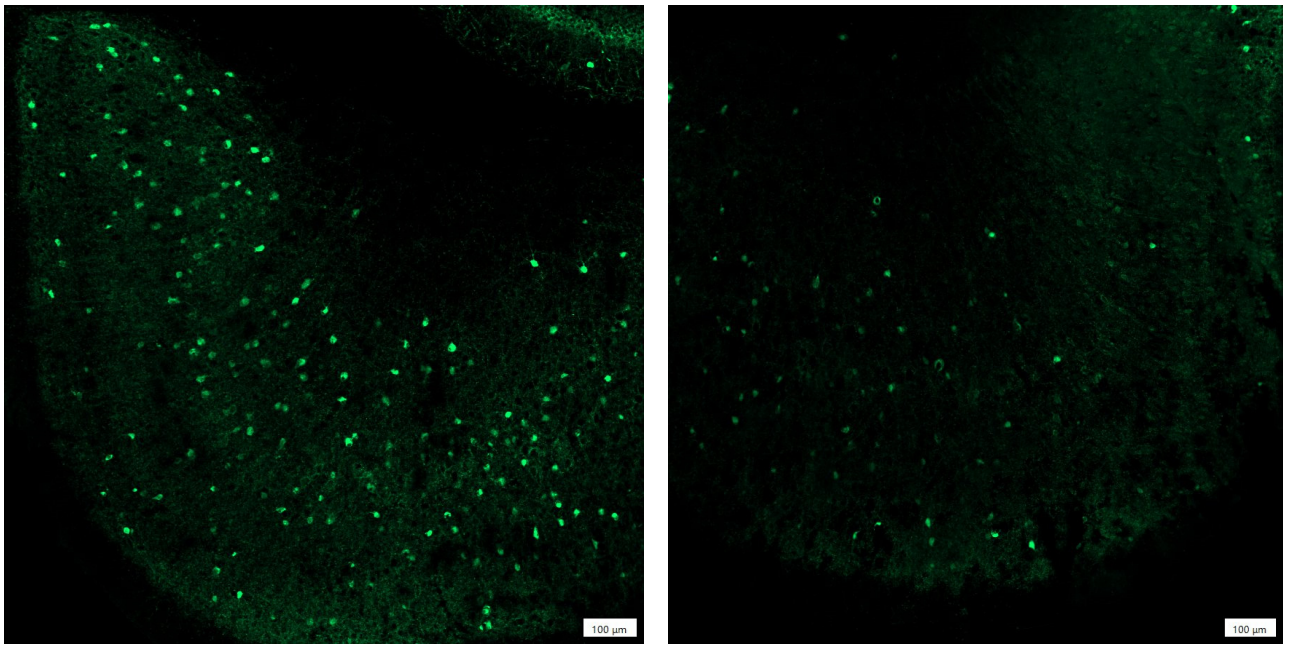

B

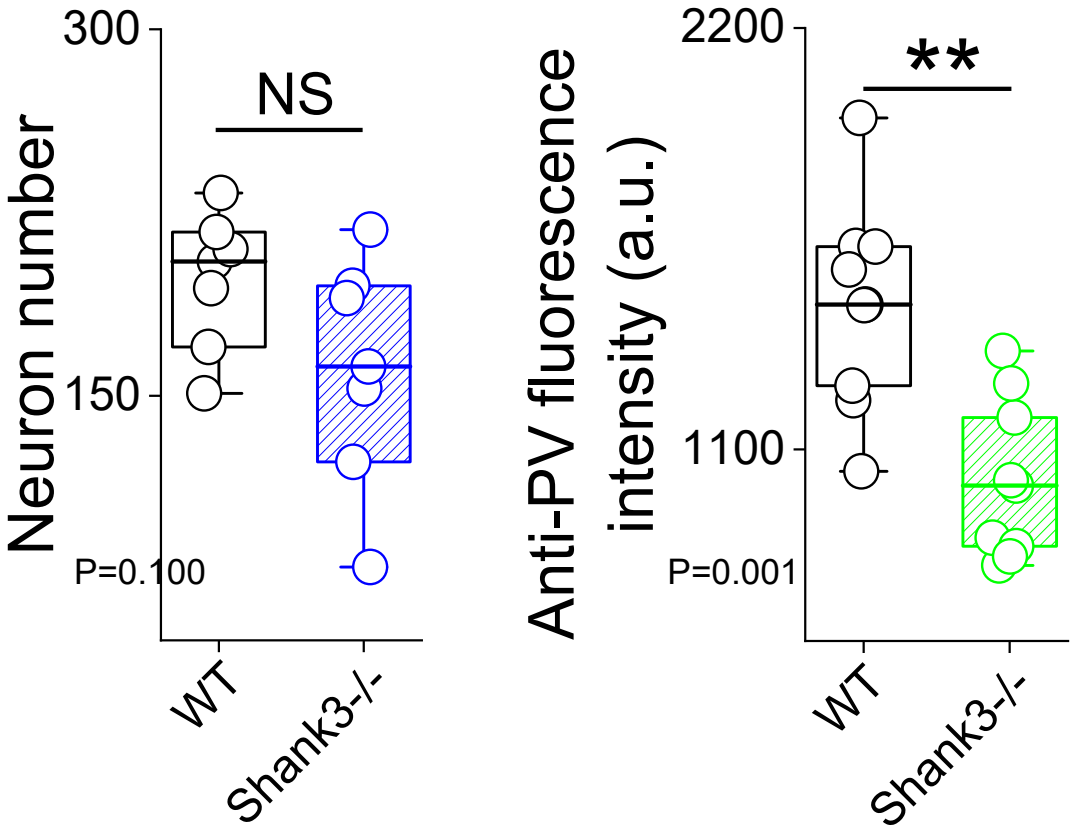

Fig. S5

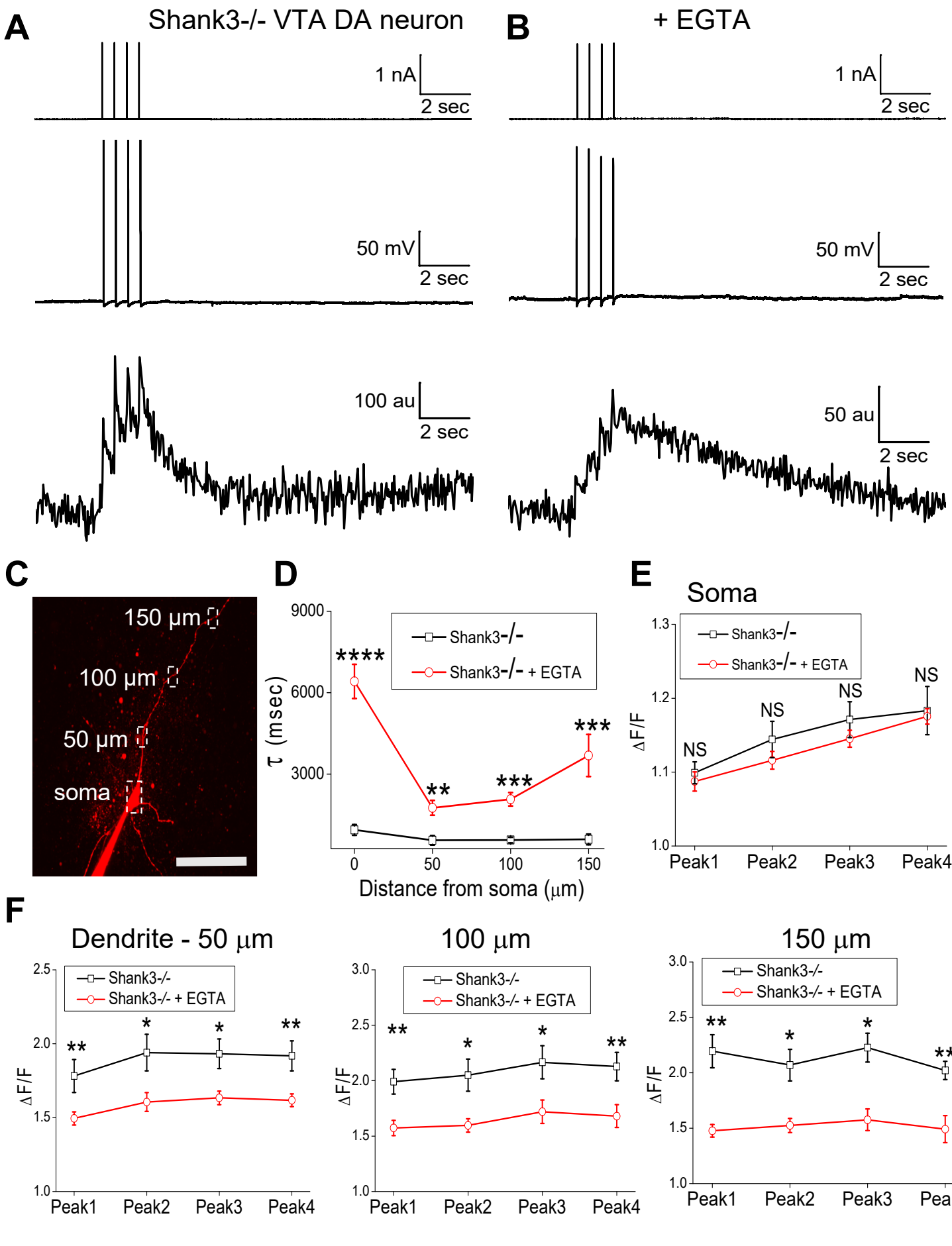

Fig. S6

A

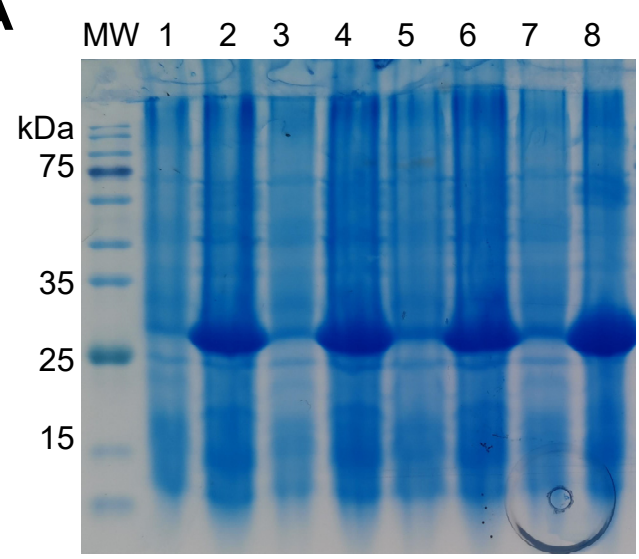

Pre-induction: 1, 3, 5, 7;
Post-induction: 2, 4, 6, 8.

B

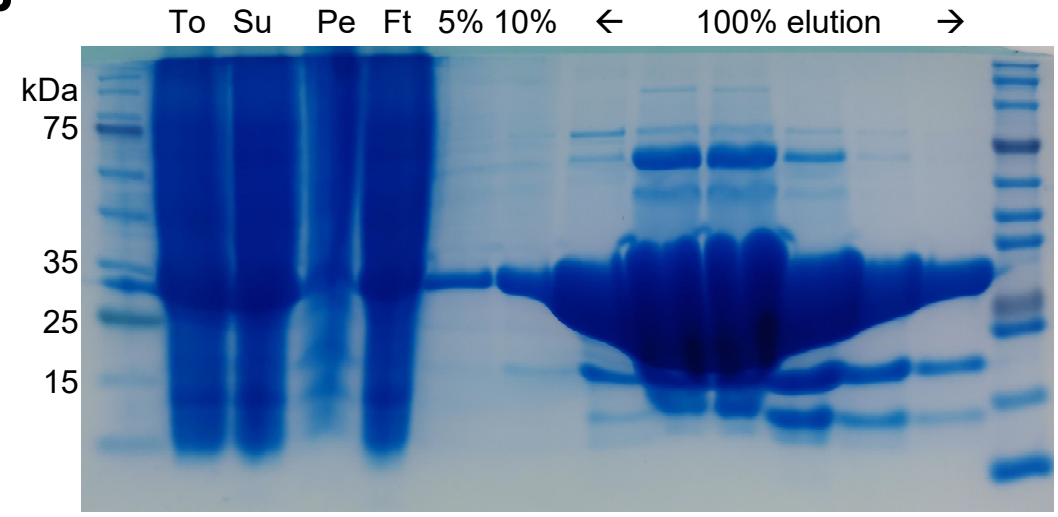

To: total
Su: supernatant
Pe: pellet
Ft: flow through

C

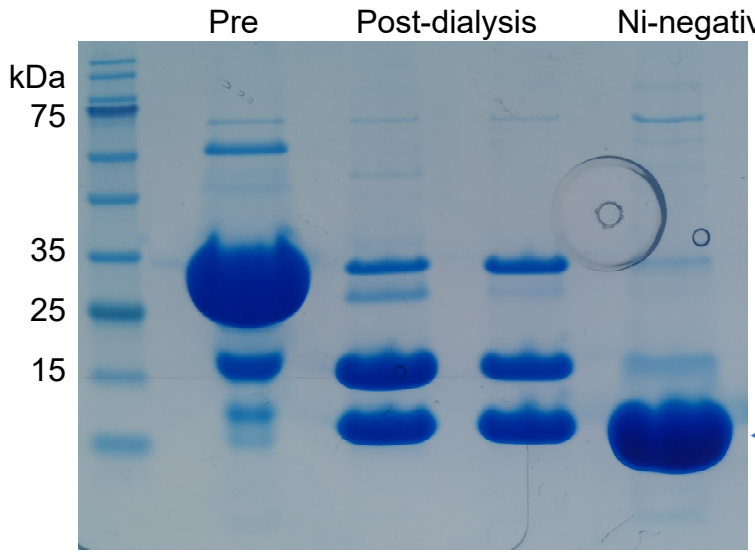

← PV目标蛋白

Fig. S7